



Dynamically Stable Walking For Humanoid Bipedal Robots Based On Walking Patterns

**Bachelor's Thesis
of**

Patrick Niklaus

At the Department of Informatics
Institute for Anthropomatics and Robotics (IAR)
High Performance Humanoid Technologies Lab (H²T)

**Primary referee: Prof. Dr.-Ing. Tamim Asfour
Advisor: Dr. Júlia Borràs Sol**

Duration: 1st July 2014 – 31st October 2014

I declare that I have developed and written the enclosed Bachelor's Thesis
completely by myself, and have not used sources or means without declaration in the text.
Karlsruhe, 31st Oktober 2014

Zusammenfassung

Fast hundert Jahre Science-Fiction haben den Begriff Roboter mit dem Bild eines mechanischen menschenähnlichen Dieners eng verbunden. In unserer modernen Welt, sind bereits große Teile unserer Produktionsketten von Robotern bestimmt. Trotzdem haben humanoide Roboter noch keinen weiterverbreiten Einzug in unseren Alltag gehalten. Ein Hauptproblem ist die Komplexität solcher Systeme. Bildverarbeitung, maschinelles Lernen, Greifen und Fortbewegung müssen in einer Maschine kombiniert werden. Jede dieser Komponenten ist für sich genommen bereits hoch komplex und ein aktuelles Forschungsthema. Eine besondere Herausforderung stellt jedoch die Fortbewegung da. Zum einen bedarf es der präzisen Koordination vieler Gelenke um zweibeiniges Laufen umzusetzen. Zum anderen ist die dynamische Beschreibung eines solchen System hoch komplex und muss deshalb stark simplifiziert werden um überhaupt handhabbar zu sein. Während andere Komponenten eines humanoiden Roboters durchaus unabhängig vom Gesamtsystem Verwendung finden, ist zweibeiniges Laufen sehr spezifisch. So können die Strategien, die für zweibeiniges Laufen entwickelt wurden, nur schwer auf andere Beinkonfigurationen übertragen werden. Einige Roboter, wie z.B. ARMAR III umgehen das Problem der zweibeinigen Fortbewegung, indem sie die Beine durch eine Plattform auf Rädern ersetzen. Das Resultat ist eine stabile Forschungsplattform. Allerdings ist die Navigation in menschlichen Umgebungen, im Vergleich zu zweibeiniger Fortbewegung, deutlich weniger flexibel.

In den letzten 20 Jahren wurden große Erfolge im Bereich es zweibeinigen Laufens erzielt. Jeder kennt die Erfolge des von HONDA entwickelten Roboters ASIMO oder die von AIST entwickelten HRP Roboter.

Frühe zweibeinige Roboter hatten einen sehr charakteristische Laufstil. Beide Füße waren immer parallel zum Boden und der Fuß wurde immer flach aufgesetzt. Damit einhergehend ist eine durchgehende Beugung der Kniegelenke. Aktuelle Robotergenerationen, z.B. HRP-4C oder WABIAN, können ein deutlich natürlicheren Laufstil umsetzen, indem sie diese Einschränkungen aufweichen und auch die Ferse und Zehen zum Laufen benutzen.

In dieser Arbeit werden die theoretischen Grundlagen zum zweibeinigen Laufen, gängige Modelle und Vereinfachungen beleuchtet. Grundlegend für hier Vorgestellten Verfahren sind sog. *Walking Patterns* (wörtlich "Laufmuster"). Aufbauend auf einer vorherigen Implementierung werden *Walking Patterns* für gerades Laufen, Laufen im Kreis und Balancieren auf einem Bein abgeleitet.

Diese *Walking Patterns* werden in einem eigens entwickelten Physiksimulator getestet. Weiter werden Stabilisatoren besprochen um Störungen auszugleichen und um *Walking Patterns* umzusetzen, die von den Annahmen der zugrunde liegenden Modellen abweichen. Zwei Verfahren werden implementiert und die Resultate vorgestellt.

Zuletzt wird ein Verfahren zum Ausgleichen von plötzlichen Störungen (Stößen) vorgestellt und die Implementierung beschrieben.

Alle Komponenten wurden in einer Software Bibliothek LIBBIPEDAL implementiert, um sie einfach in andere Softwareprojekte einbauen zu können.

Contents

1	Introduction	1
2	Models for humanoid walking	3
2.1	The Linear Inverted Pendulum Model	3
2.1.1	The inverted pendulum	3
2.1.2	Linearization	4
2.2	The Zero Moment Point	5
2.3	The Cart-Table Model	6
2.4	Multi-Body methode to calculate the ZMP	6
3	Pattern generator	8
3.1	Computing the CoM from a reference ZMP	8
3.1.1	Pattern generation as dynamic system	8
3.1.2	Controlling the dynamic system	9
3.2	Implementation	11
3.2.1	Generating foot trajectories	11
3.2.2	ZMP reference generation	12
3.2.3	ZMP Preview Control	12
3.2.4	Inverse Kinematics	13
3.2.5	Trajectory export	13
4	Stabilizing a trajectory	14
4.1	Controlling a deviation	14
4.2	Stabilizer	14
4.2.1	Reference coordinate system	15
4.2.2	Controlling the body posture	15
4.2.3	Controlling the ankle torques	16
4.2.4	Foot force difference controller	18
4.2.5	Interaction between controllers	18
4.2.6	CoM and ZMP control	19
4.3	Implementation	19
4.4	Problems	20
4.5	Alternative approach	20
5	Push recovery	21
5.1	Capture Point	21
5.2	Fall detection	22
5.3	Recovery	22
5.4	Implementation	22
6	Dynamic Simulation	23
6.1	Simulating rigid body dynamics	23
6.2	Practical challenges of physics simulations	24
6.3	Implementation	24

7 Experimental Evaluation	27
7.1 Undisturbed walking	27
7.1.1 Walking in a straight line	27
7.1.2 Walking in a circle	30
7.2 Disturbed walking	30
7.3 Push recovery	33
8 Conclusion and future work	34

1 Introduction

Nearly one hundred years of Science-Fiction have established the firm image of a mechanical humanoid servant with super human capabilities, with the term *Robot*. Today we live in a world where large parts of our production circles are already dominated by robots. Yet, widespread adoption of humanoid robots is still nowhere to be seen. One core problem of humanoid robots is their inherent complexity. Vision, cognition, manipulation and locomotion all need to be combined in one machine. While each of these problems is under active research, one has been especially resilient: Locomotion. There are multiple reasons for this. For one, locomotion is inherently complex, as a large number of joints need to be controlled precisely. The dynamics for such complex systems are hard to control, thus severe simplifications need to be made. And last but not least, the strategies to solve bipedal walking are very much tied to specific problems and not easily transferable to robots with other leg configurations. Some robots, e.g. the ARMAR III robots, circumvent it by replacing the legs with a stable base on wheels. While this yields convenient research platform, the navigation in human environments is not as natural as for full humanoid robots.

Over the last two decades a lot of progress has been made in humanoid walking. Everyone is familiar with the famous ASIMO robot developed by HONDA or the HRP robots developed by AIST which demonstrate stable walking. More recently ATLAS by Boston Dynamics shows great stability even under disturbances. Sadly, some of these platforms are closed and it is not known exactly which models are used in each robot to derive stable walking.

As the goal for bipedal walking is to be as human-like as possible, research on human walking is a great inspiration for robotic walking. While the human gait can be divided into many phases, the number of feet that are in contact with the ground is of primary interest for the stability. For walking, the ground contact alternates between both feet and one foot. These phases are called dual and single support respectively. Each step starts with a dual support phase that shifts the center of mass to the foot that supports the weight in the next step. The non-supporting foot (the *swing foot*) is then moved to the next foot hold. (See figure 1.1) The area that is in contact with the ground is not constant in each phase. Most notably at the end of the single support phase the heel is lifted. Consequently the contact changes from full sole contact to the toes. The swing foot hits the ground heel first and rotates to meet the ground while the center of mass is shifted forward.

Early robots were only able to emulate this walking style to varying degrees. A common simplification is to use a foot without movable toes. The result is a characteristic walking style, where the foot sole is

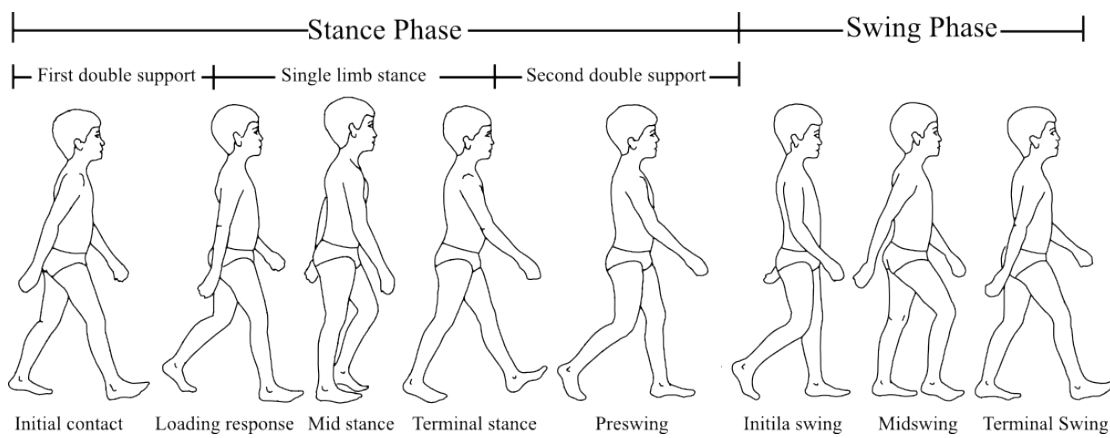


Figure 1.1: Phases of human gait. Source: Dynamics of Human Gait [1], page 9

always parallel to the ground. The most prominent example is the early ASIMO robot. However today human-like walking using the toes has been successfully demonstrated e.g. by the WABIAN-2R robot [2].

Besides the need for an adequate kinematic structure, deriving trajectories that are stable is not trivial. When talking about stability, one needs to consider two cases: *Static* and *dynamic* stability. Static stability is concerned with the stability of objects at rest (e.g. standing), while dynamical stability is concerned with the stability of objects in motion (e.g. walking). Deriving a stability criteria for the *static* case is rather simple. If the projection of center of mass to the ground is inside the support polygon, the pose is said to be *statically* stable. The support polygon is the convex hull of all points of the foot that are in contact with the ground. However dynamic stability deals with the stability of objects (e.g. in this case robots) in motion. In that case more elaborate methods need to be derived using a description of the dynamics of the robot.

There are two basic approaches to derive a trajectory for bipedal walking. On the one side there are approaches based on direct imitation of a human motion. First a human test subject is equipped with markers. The marker movements are recorded using motion capturing and mapped to corresponding markers on a humanoid model. Since the kinematic structure of a human does not map directly to the kinematic structure of a robot, the resulting trajectory needs to be adapted to the target robot. In general, only adapting the motion based on the kinematic structure will not yield a dynamically stable motion. Different weights and inertia values of the links also need to be considered. However, compensating for that might cause significant modifications of the original trajectory.

On the other side there are completely synthetic approaches. Based on simplified models of the dynamics of a humanoid robot, stability conditions are derived. Using desired foot positions or step length and walking speed as input, corresponding trajectories are derived that satisfy the given stability conditions. Most notably in this category are approaches based on the Zero Moment Point using a so called Pattern Generator. In section 2 the ZMP is derived for different simplified dynamic models. Fundamental for this approach is the insight that the dynamics of bipedal walking can be approximated sufficiently by an inverted pendulum. The model views the center of mass as the head of the pendulum, while the base is attached to the support foot. Thus the task of walking can be formalized as moving the base of the pendulum while keeping it upright.

In reality executing a trajectory that was obtained by either method is not easy. For one, the models to approximate the dynamics of a complex robot might be inaccurate. Also the environment the robot operates in might not match the assumptions of the model completely. For example, a convenient assumption is that the ground is completely flat. This is rarely the case and needs to be accounted for. Thus a stabilizer is needed to adapt the trajectory to the disturbances. Most stabilizers for established robotic platforms are closed source and very robot specific. Notably various iterations of stabilizers based on modifying an already dynamically stable pattern were proposed by Kajita and Miura et al. ([3], [4] and [5]).

While a stabilizer can deal with continuous small disturbances, a robot may encounter short but severe disturbances. These disturbances can be viewed as pushes. To recover from such disturbances, Pratt et al. established the concept of a Capture Point. Placing a foot of the robot at this point will ensure the center of mass will come to a rest. Building on this concept a recovery strategy can be derived.

This thesis presents a software framework that implements rudimentary support for each component. They are integrated into a dynamic simulation environment and evaluated experimentally.

2 Models for humanoid walking

2.1 The Linear Inverted Pendulum Model

A simple model for describing the dynamics of a bipedal robot during single support phase is the 3D inverted pendulum. We reduce the body of the robot to a point-mass at the center of mass. The support leg is replaced by a mass-less telescopic leg which is fixed at a point on the supporting foot. Initially this will yield non-linear equations that will be hard to control. However by constraining the movement of the inverted pendulum to a fixed plane, we can derive a linear dynamic system. This model is called the 3D *linear* inverted pendulum model (short *3D-LIPM*).

2.1.1 The inverted pendulum

To describe the dynamics of the inverted pendulum we are mainly interested in the effect a given actuator torque has on the movement of the pendulum.

For simplicity we assume that the base of the pendulum is fixed at the origin of the current Cartesian coordinate system. Thus we can describe the position of the inverted pendulum by a vector $c = (c_x, c_y, c_z)$. We are going to introduce an appropriate (generalized) coordinate system $q = (\theta_x, \theta_y, r)$ to get an easy description of our actuator torques: Let m be the mass of the pendulum and r the length of the telescopic leg. θ_y and θ_x describe the corresponding roll and pitch angles of the pose of the pendulum.

Now we need to find a mapping between forces in the Cartesian coordinate system and the generalized forces (the actuator torques). Let $\Phi : \mathbb{R}^3 \rightarrow \mathbb{R}^3, (\theta_x, \theta_y, r) \mapsto (x, y, z)$ be a function that maps the generalized coordinates to the Cartesian coordinates. Then the Jacobian $J_\Phi = \frac{\partial p}{\partial q}$ maps the *generalized velocities* to *Cartesian velocities*. Furthermore we know that the transpose J_Φ^T maps *Cartesian forces* $F = m(\ddot{x}, \ddot{y}, \ddot{z})$ to *generalized forces* $\Gamma = (\tau_x, \tau_y, f)$.

We write c_x, c_y and c_z in terms of our generalized coordinates to compute the corresponding Jacobian J_Φ . From the fact that the θ_y is the angle between the projection of c onto the xz -plane and c and θ_x the angle between c and the projection onto the yz plane we can derive the following equations [6]. We use $s_i = \sin(\Theta_i)$ and $c_i = \cos(\Theta_i)$ with $i \in \{x, y\}$ as a shorthand notation.

$$\begin{aligned} c_x &= r \cdot \sin \theta_y &=: r \cdot s_y \\ c_y &= -r \cdot \sin \theta_x &=: -r \cdot s_x \\ c_z &= \sqrt{r^2 - c_x^2 - c_y^2} = r \cdot \sqrt{1 - s_y^2 - s_x^2} \end{aligned} \quad (2.1)$$

From which we can compute the Jacobian by partial derivation:

$$J = \frac{\partial p}{\partial q} = \begin{pmatrix} 0 & r \cdot c_y & s_y \\ -r \cdot c_x & 0 & s_x \\ \frac{2 \cdot r \cdot s_y c_y}{\sqrt{1 - s_y^2 - s_x^2}} & \frac{2 \cdot r \cdot s_x c_x}{\sqrt{1 - s_y^2 - s_x^2}} & \sqrt{1 - s_y^2 - s_x^2} \end{pmatrix} \quad (2.2)$$

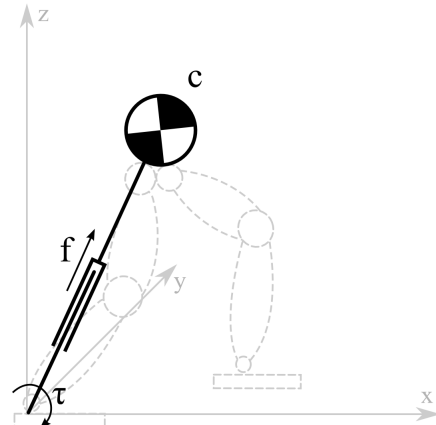


Figure 2.1: The 3D-LIMP

Using the gravity force $f_g = (0, 0, -m \cdot g)^T$ and the equation of motion as given by

$$\begin{aligned} F &= (J^T)^{-1} \Gamma + f_g \\ m \cdot \begin{pmatrix} \ddot{c}_x \\ \ddot{c}_y \\ \ddot{c}_z \end{pmatrix} &= (J^T)^{-1} \begin{pmatrix} \tau_x \\ \tau_y \\ f \end{pmatrix} + \begin{pmatrix} 0 \\ 0 \\ -m \cdot g \end{pmatrix} \end{aligned} \quad (2.3)$$

and equations 2.2 and 2.1 we can derive the following equations:

$$m(-z\ddot{c}_y + y\ddot{c}_z) = \frac{\sqrt{1 - s_y^2 - s_x^2}}{c_x} \cdot \tau_x + mgc_y \quad (2.4)$$

$$m(z\ddot{c}_x - x\ddot{c}_z) = \frac{\sqrt{1 - s_y^2 - s_x^2}}{c_y} \cdot \tau_y + mgc_x \quad (2.5)$$

The terms of the left-hand side are not linear. To remove that non-linearity we are going to use the *linear* inverted pendulum model.

2.1.2 Linearization

In a man-made environment it is fair to assume that the ground a robot will walk on can be approximated by a slightly sloped plane. In most cases it can even be assumed that there is no slope at all.

The basic assumption in the next section will be that the CoM will have a *constant displacement* with regard to our ground plane. Thus we can constrain the movement of the CoM to a plane that is parallel to the ground plane. Note that these assumption is, depending on the walking speed, only approximately true for human walking as shown by Orendurff et al. [7]. For slow to fast walking (0.7 m/s and 1.6 m/s respectively) the average displacement in z -direction was found to be between 2.7 cm and 4.81 cm. While the walking patterns generated based on the LIP-model will guarantee dynamic stability, they might not look natural with regard to human walking.

We are going to constrain the z -coordinate of our inverted pendulum to a plane with normal vector $(k_x, k_y, -1)$ and z -displacement z_c :

$$c_z = k_x \cdot c_x + k_y \cdot c_y + z_c \quad (2.6)$$

Subsequently the second derivative of c_z can be described by:

$$\ddot{c}_z = k_x \cdot \ddot{c}_x + k_y \cdot \ddot{c}_y \quad (2.7)$$

Substituting 2.6 and 2.7 into the equations 2.4 and 2.5 yields the following equations:

$$\ddot{c}_x = \frac{g}{z_c} c_x + \frac{k_y}{z_c} (c_x \ddot{c}_y - \ddot{c}_x c_y) + m z_c \cdot \tau_y \cdot \frac{\sqrt{1 - s_y^2 - s_x^2}}{c_y} \quad (2.8)$$

$$\ddot{c}_y = \frac{g}{z_c} c_y - \frac{k_x}{z_c} (c_x \ddot{c}_y - \ddot{c}_x c_y) - m z_c \cdot \tau_x \cdot \frac{\sqrt{1 - s_y^2 - s_x^2}}{c_x} \quad (2.9)$$

The term $c_x \ddot{c}_y - \ddot{c}_x c_y$ that is part of both equations is still causing the equations to be non-linear. To make these equations linear we will assume that our ground plane has no slope, thus $k_x = k_y = 0$ and the non-linear terms will vanish.

Another problem is that the actuator torques τ_x and τ_y both have non-linear factors $\frac{\sqrt{1 - s_y^2 - s_x^2}}{c_x}$ and $\frac{\sqrt{1 - s_y^2 - s_x^2}}{c_y}$ respectively. This can be solved by substituting with the following *virtual inputs*:

$$\tau_x \cdot \frac{\sqrt{1 - s_y^2 - s_x^2}}{c_x} = u_x \quad (2.10)$$

$$\tau_y \cdot \frac{\sqrt{1 - s_y^2 - s_x^2}}{c_y} = u_y \quad (2.11)$$

Which yields our final description of the dynamics:

$$\ddot{c}_x = \frac{g}{z_c} c_x + \frac{u_x}{m z_c} \quad (2.12)$$

$$\ddot{c}_y = \frac{g}{z_c} c_y - \frac{u_y}{m z_c} \quad (2.13)$$

As outlined in [6] the inputs u_y and u_x are generally set to zero. Thus the 3D-LIMP has no input torque. This is desirable, as the torque that can be applied on the ankle joints is limited and it makes sense to reserve the torque for correcting disturbances.

2.2 The Zero Moment Point

The Zero Moment Point is virtual point on the floor that can be used to derive dynamically stable walking. If the support foot (or support feet) have flat ground contact, the walking trajectory is dynamically stable if the ZMP is strictly inside the support polygon. If the ZMP is on the border of the support polygon, the trajectory can be dynamically unstable. By deriving a control scheme that constrains the ZMP to be strictly inside the support polygon, we can use the ZMP to generate dynamically stable trajectories.

For flat ground contact of our support foot with the floor the ZMP corresponds with the position of the center of pressure (CoP). Indeed, some authors (notably Pratt) prefer to use the term CoP instead of ZMP. In the context of this thesis, we will use the term ZMP.

The CoP (and in flat ground contact the ZMP) of an object in contact with the ground can be computed as the sum of all contact points p_1, \dots, p_n weighted by the forces in z -direction f_{1z}, \dots, f_{nz} that is applied:

$$p := \begin{pmatrix} p_x \\ p_y \\ p_z \end{pmatrix} = \frac{\sum_{i=1}^N p_i f_{iz}}{\sum_{i=1}^N f_{iz}} \quad (2.14)$$

An important fact (and the origin of its name) is that there are no torques around the x and y axis at the ZMP:

$$\tau = \sum_{i=1}^N (p_i - p) \times f_i \quad (2.15)$$

Splitting that up into each component using the definition of the cross product yields:

$$\tau_x = \sum_{i=1}^N (p_{iy} - p_y) f_{iz} - \underbrace{(p_{iz} - p_z)}^{=0} f_{iy} \quad (2.16)$$

$$\tau_y = \sum_{i=1}^N \underbrace{(p_{iz} - p_z)}^{=0} f_{ix} - (p_{ix} - p_x) f_{iz} \quad (2.17)$$

$$\tau_z = \sum_{i=1}^N (p_{ix} - p_x) f_{iy} - (p_{iy} - p_y) f_{ix} \quad (2.18)$$

Since we have flat ground contact, all contact points have the same z -coordinate as the ZMP, thus we can simplify τ_x and τ_y to:

$$\tau_x = \sum_{i=1}^N (p_{iy} - p_y) f_{iz} = \sum_{i=1}^N (p_{iy} f_{iz}) - (\sum_{i=0}^N f_{iz}) \cdot p_y \quad (2.19)$$

$$\tau_y = \sum_{i=1}^N -(p_{ix} - p_x) f_{iz} = \sum_{i=1}^N -(p_{ix} f_{iz}) + (\sum_{i=0}^N f_{iz}) \cdot p_x \quad (2.20)$$

Furthermore, we can use the corresponding components p_x and p_y from the definition of the ZMP 2.14 and substitute them in the equations 2.19 and 2.20.

This will yield: $\tau_x = \tau_y = 0$. Please note that τ_z will in general not be zero, nonetheless in case of straight walking it is often assumed to be zero as well.

2.3 The Cart-Table Model

The Cart-Table model is used to compute the resulting ZMP from an CoM motion. The model consists of an infinitely large mass-less table of height z_c , while the foot of the table has the shape of the support polygon. Given a frictionless cart with mass m at position $c = (c_x, c_y, c_z)$ that moves on the table we can compute the resulting ZMP $p = (p_x, p_y, p_z)^T$ in the support foot. Please note that the 3D-dimensional model is equivalent to having two independent tables with two carts each in the xz - and yz -plane respectively. First of all, lets compute the torque τ_x and τ_y around the x-axis and y-axis at the ZMP on the support foot.

$$\tau_y = \underbrace{-mg(c_x - p_x)}_{\text{torque due to gravity}} + \underbrace{m\ddot{x} \cdot z_c}_{\text{torque due to acceleration of cart}} \quad (2.21)$$

$$\tau_x = -mg(c_y - p_y) + m\ddot{y} \cdot z_c \quad (2.22)$$

Please note the similarity to the equations 2.13 and 2.12 when assuming the base of the pendulum is located at p . If we now use the property of the ZMP that the torque around the x and y -axis is zero, we can solve for the ZMP position p :

$$p_x = c_x - \frac{z_c}{g} \ddot{c}_x \quad (2.23)$$

$$p_y = c_y - \frac{z_c}{g} \ddot{c}_y \quad (2.24)$$

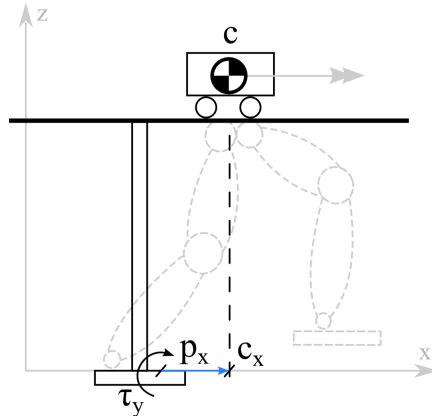


Figure 2.2: The Cart-Table model.

2.4 Multi-Body methode to calculate the ZMP

Besides the simplified Cart-Table Model, there also exists an exact method to calculate the resulting ZMP from the movement of several connected rigid bodies.

Let c_i be the CoM position and m_i the mass of the i -th body ($i \in \{1, \dots, k\}$). Then, as derived in [8] (p. 374), the total linear momentum \mathcal{P} can be calculated by:

$$\mathcal{P} = \sum_{j=1}^k m_j \cdot \dot{c}_j \quad (2.25)$$

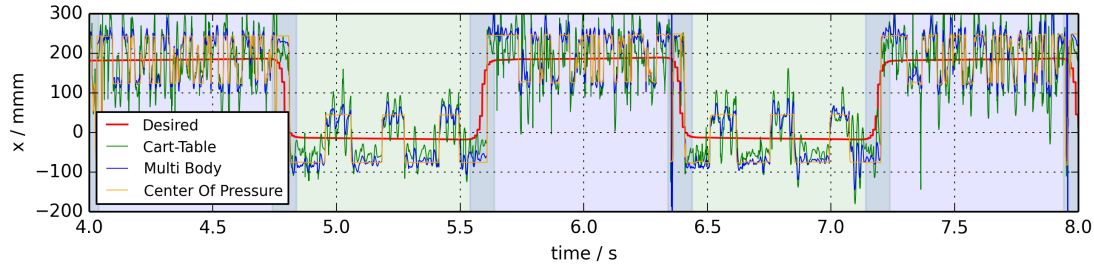


Figure 2.3: Comparison of the Cart-Table and Multi-Body to estimate the realized ZMP during walking simulation.

If ω_i is the angular momentum and R_i is the rotational part of the reference frame of the i -th body and I_i the inertia tensor in that reference frame, the total angular momentum \mathcal{L} can be calculated by:

$$\mathcal{L} = \sum_{j=1}^k c_j \times (m_j \dot{c}_j) + R_j I_j R_j^T \omega_j \quad (2.26)$$

If we denote the total mass of the robot with M and the gravity vector with g we can express the change of linear momentum if a force f is applied to the body as:

$$\dot{\mathcal{P}} = Mg + f \quad (2.27)$$

And subsequently the change in angular momentum if a torque τ is applied:

$$\dot{\mathcal{L}} = c \times Mg + \tau \quad (2.28)$$

To calculate the resulting torque τ_{ZMP} around the ZMP located at p we can use:

$$\tau_{ZMP} = \tau + (0 - p) \times f = \tau - p \times f \quad (2.29)$$

If we solve equation 2.27 for f and 2.28 for τ and substitute them in 2.29 this yields the following equation:

$$\tau_{ZMP} = \dot{\mathcal{L}} - c \times Mg - p \times (\dot{\mathcal{P}} - Mg) \quad (2.30)$$

Since we know that the torque around the ZMP is zero around the x and y axis we can apply the definition of the cross product and solve for the ZMP position:

$$p_x = \frac{Mgx + p_z \dot{\mathcal{P}}_x - \dot{\mathcal{L}}_y}{Mg + \dot{\mathcal{P}}_z} \quad (2.31)$$

$$p_y = \frac{Mgy + p_z \dot{\mathcal{P}}_y - \dot{\mathcal{L}}_x}{Mg + \dot{\mathcal{P}}_z} \quad (2.32)$$

Both equations are dependent on p_z . If we assume the robot walks on a flat floor, we can set $p_z = 0$.

See figure 2.3 to get an idea how much the Multi-Body ZMP derives from the estimation using the Cart-Table Model.

3 Pattern generator

To generate a walking pattern for a bipedal robot two basic approaches are common:

1. Generate (or modify) foot trajectories that realizes a prescribed trajectory of the CoM.
2. Generate a CoM trajectory for prescribed foot trajectories.

The first approach is generally used for implementing pattern generators solely based on the 3D-LIP model. [6] The second approach is more versatile, since it is easy to incorporate constraints of our environment (e.g. only limited foot holds) in the input of the pattern generator. However care must be taken while choosing adequate step width and step length parameters for the foot trajectory, so that they can actually be realized by the robot. The pattern generator proposed by Kajita et al. [9] based on Preview Control realizes the second approach. We will discuss the theoretical background of this pattern generator here in more detail, since all patterns that we used were generated that way.

3.1 Computing the CoM from a reference ZMP

As we saw in the section 2.3 it is easy to compute the resulting ZMP given the CoM and its acceleration. However, for generating the walking pattern, we want to compute the CoM trajectory from a given ZMP. If you rearrange the equations 2.23 and 2.24 you see that we have to solve a second order differential equations:

$$c_x = \frac{z_c}{g} \cdot \ddot{c}_x + p_x \quad (3.1)$$

$$c_y = \frac{z_c}{g} \cdot \ddot{c}_y + p_y \quad (3.2)$$

There are several ways to solve these differential equations, for example by transforming them to the frequency-domain. This however would mean that the ZMP trajectory needs to be transformed to the frequency domain as well, e.g. using Fast Fourier Transformation. This has two main problems:

1. It has a significant computational overhead (for FFT the additional runtime would be in $O(n \log n)$).
2. We need to know the whole ZMP trajectory in advance.

Instead Kajita et al. chose to define a dynamic system in the time domain that describes the CoM movement.

3.1.1 Pattern generation as dynamic system

For simplicity we will only focus on the dynamic description of one dimension, as the other one is analogous. To transform the equations to a strictly proper dynamical system, we need to determine the state vector of our system. For the Cart-Table Model it suffices to know the position, velocity and acceleration of the cart, i.e. the CoM. Thus the state-vector is defined as $x = (c_x, \dot{c}_x, \ddot{c}_x)$. We can define the evolution of the state vector as follows:

$$\frac{d}{dt} \begin{pmatrix} c_x \\ \dot{c}_x \\ \ddot{c}_x \end{pmatrix} = \underbrace{\begin{pmatrix} 0 & 1 & 0 \\ 0 & 0 & 1 \\ 0 & 0 & 0 \end{pmatrix}}_{=:A_0} \cdot \begin{pmatrix} c_x \\ \dot{c}_x \\ \ddot{c}_x \end{pmatrix} + \underbrace{\begin{pmatrix} 0 & 0 & 0 \\ 0 & 0 & 0 \\ 1 & 0 & 0 \end{pmatrix}}_{=:B_0} u \quad (3.3)$$

The jerk of the CoM was introduced as an input $u_x = \frac{d}{dt} \ddot{c}_x$ into the dynamic system. We use equation 2.23 to calculate the actual output of the dynamic system the resulting ZMP, that will be controlled:

$$p_x = \begin{pmatrix} 1 & 0 & \frac{-z_c}{g} \end{pmatrix} \cdot \begin{pmatrix} c_x \\ \dot{c}_x \\ \ddot{c}_x \end{pmatrix} \quad (3.4)$$

Using this formulation of the dynamic system we need to derive the evolution of our state vector using the state-transition matrix. Since our input ZMP trajectory will consist of discrete samples at equal time intervals T we define the discrete state as $x[k] := x(k \cdot T)$. Please note that this system is a linear time-invariant system (LTI), and both matrices A_0 and B_0 are constant. We can therefore use the standard approach to solve these systems using the equation:

$$x(t) = e^{A_0 \cdot (t-\tau)} x(\tau) + \int_{\tau}^t e^{A_0 \cdot (t-\lambda)} B_0 u(\lambda) d\lambda \quad (3.5)$$

In our discrete case that becomes:

$$x[k+1] = e^{A_0 \cdot ((k+1)T - kT)} x[k] + \int_{kT}^{(k+1)T} e^{A_0 \cdot ((k+1)T - \lambda)} B_0 u(\lambda) d\lambda \quad (3.6)$$

$$= e^{A_0 \cdot T} x[k] + \left(\int_{kT}^{(k+1)T} e^{A_0 \cdot ((k+1)T - \lambda)} d\lambda \right) \cdot B_0 u[k] \quad (3.7)$$

$$= e^{A_0 \cdot T} x[k] + \left(\int_T^0 e^{A_0 \cdot \lambda} d\lambda \right) \cdot B_0 u[k] \quad (3.8)$$

Keep in mind that $u(\lambda) = u[k], \lambda \in (kT, (k+1)T)$ so we can move it outside of the integral. Let us first compute a general solution for the matrix exponential $e^{A_0 \cdot t}$. It is easy to see that A_0 is nilpotent and $A_0^3 = 0$, thus the computation simplifies to the following:

$$e^{A_0 t} := \sum_{i=0}^{\infty} \frac{(A_0 \cdot t)^i}{i!} = I + A_0 \cdot t + A_0^2 \cdot \frac{t^2}{2} + 0 = \begin{pmatrix} 1 & t & \frac{t^2}{2} \\ 0 & 1 & t \\ 0 & 0 & 1 \end{pmatrix} \quad (3.9)$$

Using this solution computing the integral in 3.6 is quite easy:

$$\int_T^0 e^{A_0 \cdot \lambda} d\lambda = - \int_0^T \begin{pmatrix} 1 & t & \frac{t^2}{2} \\ 0 & 1 & t \\ 0 & 0 & 1 \end{pmatrix} dt = - \left[\begin{pmatrix} t & \frac{t^2}{2} & \frac{t^3}{6} \\ 0 & t & \frac{t^2}{2} \\ 0 & 0 & t \end{pmatrix} \right]_0^T = \begin{pmatrix} T & \frac{T^2}{2} & \frac{T^3}{6} \\ 0 & T & \frac{T^2}{2} \\ 0 & 0 & T \end{pmatrix} \quad (3.10)$$

Substituting the results in 3.6 yields:

$$x[k+1] = \underbrace{\begin{pmatrix} 1 & T & \frac{T^2}{2} \\ 0 & 1 & T \\ 0 & 0 & 1 \end{pmatrix}}_{=:A} x[k] + \underbrace{\begin{pmatrix} \frac{T^3}{6} \\ \frac{T^2}{2} \\ T \end{pmatrix}}_{=:B} \cdot u_x[k] \quad (3.11)$$

3.1.2 Controlling the dynamic system

To control this dynamic system we need to determine an adequate control input u_x to realize the reference ZMP trajectory. A performance index J_x for a given control input u_x is needed to formalize what a “good” control input would be. A naive performance index could be:

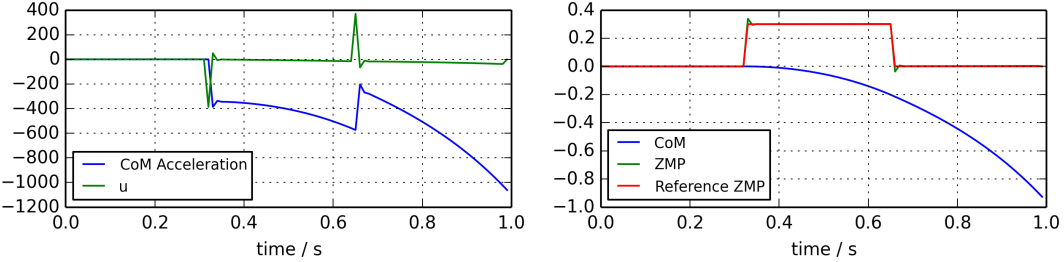


Figure 3.1: ZMP control based on the performance index described by equation 3.12.

$$J_x[k+1] := (p_x^{ref}[k+1] - p_x[k+1])^2 \quad (3.12)$$

To minimize it, we need to find u_x for which $p_x = p_x^{ref}$. By substituting $p_x[k+1]$ with 3.4 and $x[k+1]$ with 3.11 this yields:

$$u_x[k] = \frac{p_x^{ref}[k+1] - C \cdot A \cdot x[k]}{C \cdot B} = \frac{p_x^{ref}[k+1] - (1, T, \frac{1}{2}T^2 - \frac{z_c}{g}) \cdot x[k]}{\frac{1}{6}T^3 - \frac{z_c}{g}T} = \frac{p_x^{ref}[k+1] - p_x[k] - T\dot{c}_x[k] - \frac{1}{2}T^2\ddot{c}_x[k]}{\frac{1}{6}T^3 - \frac{z_c}{g}T} \quad (3.13)$$

To analyze the behavior of this control law for u_x we simulate the rapid change of reference ZMP when changing the support foot.

As can be seen, the reference ZMP is perfectly tracked. However, the CoM does not behave as expected. To achieve the required ZMP position the CoM will be *accelerated indefinitely* in the opposite direction. Clearly this is not desired and will lead to falling of a real robot. A more sophisticated performance index is needed. To eventually reach a stable state at which the CoM comes to rest, the performance index should include a state feedback. Also note the large jerk that is applied to the system when the reference ZMP position changes rapidly. In a real mechanical system large jerks will lead to oscillations, which will disturb the system. Thus the performance index should also try to limit the applied jerk.

Another problem is caused by the very nature of a controller: The controller starts to act *after* we have a deviation from our reference ZMP trajectory. Trying to reduce this lag as much as possible can lead to very high velocities, which might not be realizable by motors of a robot. However we have at least limited knowledge of the future reference trajectory. This knowledge can be leveraged by using Preview Control, which considers the next N time steps for computing the performance index.

Kajita et al. use a performance index proposed by Katayama et al. [10] to solve all of the problems above:

$$J_x[k] = \sum_{i=k}^{\infty} Q_e e[i]^2 + \Delta x[i]^T Q_x \Delta x[i] + R \Delta u_x[i]^2 \quad (3.14)$$

Q_e is the error gain, Q_x a symmetric non-negative definite matrix (typically just a diagonal matrix) to weight the components of $\Delta x[i]$ differently and $R > 0$. Conveniently Katayama also derived an optimal controller for this performance index, which is given by:

$$u[k] = -G_i \sum_{i=0}^k e[k] - G_x x[k] - \sum_{j=1}^N G_p p_x^{ref}[k+j] \quad (3.15)$$

The gains G_i, G_x, G_p , can be derived from the parameters of the performance index. Since the calculation is quite elaborate we refer to the cited article by Katayama p. 680 for more details.

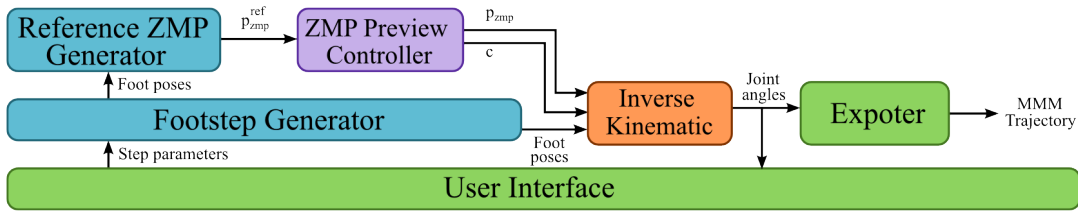


Figure 3.2: Architecture of the pattern generator

3.2 Implementation

To generate walking patterns based on the ZMP Preview Control method, the approach from Kajita was implemented in LIBBIPEDAL, a shared library that contains all walking related algorithms. A front-end was developed to easily change parameters, visualize and subsequently export the trajectory to the MMM format. The implementation was build on a previous implementation, which was refactored, extended and tuned with respect to results from the dynamics simulation. The pattern generator makes extensive usage of SIMOX VIRTUALROBOT, for providing a model of the robot and the associated task of computing the forward- and inverse kinematics.

Generating a walking pattern consists of multiple steps. First the foot positions are calculated. These are used to derive the reference ZMP trajectory which is fed into the ZMP Preview Controller. From that the CoM trajectory is computed. The CoM trajectory and feet trajectories are then used to compute the inverse kinematics. The resulting joint trajectory is displayed in the visual front-end and can be exported. Each step is contained in dedicated modules that can be easily replaced, if needed. We will outline the implementation of each module separately.

3.2.1 Generating foot trajectories

To generate the foot trajectories several parameters are needed:

Step height h Maximum distance between the foot sole and the floor

Step length l Distance in anterior direction (y -axis) between the lift-off point and the touch-down point

Step width w Distance in lateral direction (x -axis) between both TCP on the feet

Single support duration t_{ss} Time the weight of the robot is only supported by exactly one foot

Dual support duration t_{ds} Time the weight of the robot is supported by both feet

See figure 3.3 for the values used to generate the trajectories using a model of the ARMAR IV robot.

Walking straight

Since the foot trajectories of humanoid walking have a cyclic nature, we only need three different foot trajectories that can be composed to arbitrarily long trajectories: Two transient trajectories for the first and last step respectively and a cyclic motion that can be repeated indefinitely. We can use the same trajectories for both feet, as they are geometrically identical. Each foot trajectory starts with swing phase

h	0.1 m
l	0.3 m
w	0.2 m
t_{ss}	0.7 s
t_{ds}	0.1 s

Figure 3.3: Default parameters used for generating a walking trajectory.

and ends with a resting phase. The trajectory in y and z direction is computed by a 5th order polynomial that assures the velocities and accelerations are approaching zero at the lift-off and touch-down point. The first and last step only have half of the normal step length, since the trajectory is starting and ending from a dual support stance, where both feet are placed parallel to each other. Each trajectory is encoded as a $6 \times N$ matrix, where N is the number of samples. A sample period of $T = 10ms$ was used. Each column contains Cartesian coordinates and roll-pitch-yaw angles.

Walking on a circle

Much of the general structure of the foot trajectory remains the same as for walking straight. However instead of specifying the step length, it is implicitly given by the segment of the circle that should be traversed and the number of steps. So extra care needs to be taken to specify enough steps so that the generated foot positions are still reachable. Each foot needs to move on a circle with radius $r_{inner} = r - \frac{w}{2}$ or $r_{outer} = r + \frac{w}{2}$, depending on which foot lies in the direction of the turn. The movement in z -direction remains unaffected. The movement in the xy -plane is transformed to follow the circle for the specific foot. The same polynomial that was previously used for the y -direction is now used to compute the angle on the corresponding circle and the x and y coordinates are calculated accordingly. The foot orientation is computed from the tangential (y -axis) and normal (x -axis) of the circle the foot follows.

Balancing on one foot

To test push recovery from single support stance a special pattern was needed. Another footstep planer was implemented that generates a trajectory for standing on one foot. Starting from dual support stance, the swing leg is moved in vertical direction until the usual step height is achieved. Additionally the foot is moved in lateral direction to half the step width. This reduces the necessary upper body tilt to compensate the imbalance. For the last step the inverse movement is performed to get back into dual support stance. This method could be extended to walking by setting the next support foot in a straight line before the current support foot. The swing foot would need to be moved in an arc in lateral direction to avoid self-collisions.

3.2.2 ZMP reference generation

As an input for the ZMP Preview Control, we need a reference ZMP movement that corresponds with the foot trajectory. The reference generator receives a list of intervals associated with the desired support stance and foot positions as input. In single support phase, the reference generator places the ZMP in the center of the support polygon of the corresponding foot. Since the support polygon is convex, the center is the furthest point away from the border of the polygon. This should guarantee a maximum stability with regard to possible ZMP errors. In dual support phase, the reference generator shifts the ZMP from the previous support foot to the next support foot. Kajita et al. suggest using a polynomial to interpolate the ZMP positions between the feet. However a simple step function $\sigma(t) = \begin{cases} p_1 & t \leq t_0 \\ p_2 & t > t_0 \end{cases}$ seems to suffice as well. Since the touch-down of the swing foot might have a small lag, it is important that t_0 is the middle of the dual support phase. This assures we do not start to move the ZMP too early.

3.2.3 ZMP Preview Control

This module implements the method described by Kajita et al. [9] and uses the method outlined by Katayama et al. [10] to compute the optimal control input $u[k]$. Since it is computational feasible, the preview period consists of the full reference trajectory. For an online usage of this method, this could be reduced to a much smaller sample size, e.g. only preview one step ahead. Using the system dynamics described by 3.11 the CoM trajectory, velocity and acceleration can be computed. The implementation makes heavy use of EIGEN, a high performance linear algebra framework that uses SIMD instructions

to speed up calculations. Thus thus a calculation time of 6.2s could be achieved to calculate ten steps (about 1000 samples), including the inverse kinematics.

3.2.4 Inverse Kinematics

Using the foot trajectories and CoM trajectory the resulting joint angles need to be calculated. Since the used kinematic model has a total of 35 degrees of freedom, we need to reduce the number of joints that are used for the IK to a sensible value. For walking only the joints of the legs and both the torso roll and pitch joints are used. All other joints are constrained to static values that will not cause self-collisions (e.g. the arms are slightly extended and do not touch the body). For computing the IK additional constraints were added to make sure the robot has a sensible pose: The chest should always have an upright position and the pelvis should always be parallel to the floor. To support non-straight walking, the pelvis and chest orientation should also follow the walking direction. Thus the following method to compute the desired chest and pelvis orientation is used:

1. Compute walking direction y' as mean of y-axis of both feet and normalize: $y' := \frac{y_{left} + y_{right}}{|y_{left} + y_{right}|}$
2. Both should have an upright position $z' := (0, 0, 1)^T$
3. Compute x' as the normal to both vectors: $x' := y' \times z'$
4. Pose R' is given by $R' = (x', y', z')$

A special property of the model that was used for computing the inverse kinematics, is that TCP of the left leg was chosen as root node. Since we can specify the root position freely, that removes the need of solving for the left foot pose. Thus, the inverse kinematics needs to solves for the following goals:

1. Chest orientation
2. Pelvis orientation
3. CoM position
4. Right foot pose

A hierarchical solver was used to solve the inverse kinematics for these goals in the given order. It was observed that specifying a good target height for the CoM is of utmost importance for the quality of the IK. For the ARMAR IV model that was used here, a height of 0.86 m yielded the best results.

3.2.5 Trajectory export

The trajectory was exported in open MMM trajectory format. The format was extended to export additional information useful for debugging and controlling the generated trajectory. Besides the joint values and velocities the trajectory also includes the CoM and ZMP trajectory. Also, information about the current support phase is saved. For convenience, the pose of chest, pelvis, left and right foot are exported as homogeneous matrices as well. This saves the additional step of computing them again for the stabilizer and also eliminates an additional error source while debugging.

4 Stabilizing a trajectory

While executing a trajectory there are several sources of errors that will make it necessary to correct the trajectory. We can divide them in about three main classes:

Disturbances of the environment: The models pattern generators use, make some assumptions about the environment they operate in. Most prominently the 3D-LIMP assumes the floor is completely flat and has no slope. Also we assume we can navigate without colliding with other objects. Any environment that deviates from these assumptions can be seen as a disturbance.

Disturbances due to simulation errors: Physical simulations often make a trade-off between speed and simulation accuracy. Thus the simulation might not always behave as it was modeled during calculating the pattern, or as it would behave in reality.

Disturbances due to errors of the method: Often pattern generators use simplified models of the dynamics involved to derive generation scheme. For example the pattern generator that was used here assumes the ZMP behaves as the cart-table-model predicts. However, the realized ZMP can substantially deviate.

4.1 Controlling a deviation

When using a ZMP based control scheme to derive a walking pattern it seems natural to check for deviations of the actual ZMP from the goal ZMP. However a deviation from the reference ZMP does not necessarily mean we will see any disturbance. As long as the ZMP remains inside the support polygon the trajectory can be executed as planned. As we saw in 3.1.2 it is entirely possible to realize the reference ZMP while being in an overall state that deviates significantly from the state we assumed while generating the pattern. Thus we also need to check for a deviation in the trajectory of our CoM. A common approach to correct for CoM position is to control the pose of the chest frame of the robot. This only works if a significant part of the mass of a robot is located in the upper body and arms. Luckily for most humanoid robots this is the case.

4.2 Stabilizer

We chose a stabilizer proposed by Kajita et al. in their 2010 paper. [3] The stabilizer only needs the joint trajectory of the walking pattern augmented with a desired ZMP trajectory. This allows the stabilizer to use patterns that were generated synthetically, e.g. by a pattern generator, or patterns that are the results of (adapted) motion capturing. The method proposed by Kajita does not need a torque controlled robot, but works with position control. This was very important for the selection of this stabilizer. The underlying simulation engine BULLET only supports velocity controlled motors, consequently the torque can not be controlled directly.

The controller works by attaching control frames to specific points on the robot. The reference position of these frames can be calculated from the input trajectory using forward kinematics. To compensate a disturbance the orientation of a reference frame is modified. The modified reference frames are then converted to the modified joint angles by the inverse kinematics.

In the remainder of this chapter we will use the superscript d to denote reference values and the subscript $*$ to denote modified values. For this approach four control frames were selected. The chest to modify the body posture, the feet to modify the ankle torque and the pelvis to realize as natural hip position.

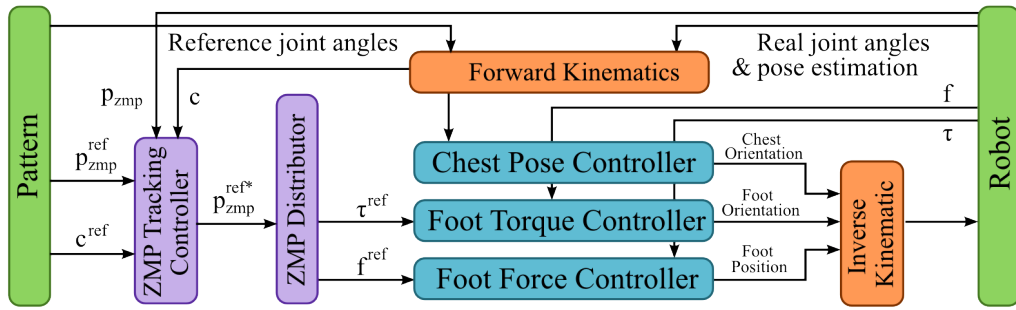


Figure 4.1: Architecture of the stabilizer

4.2.1 Reference coordinate system

To control the ZMP and CoM it is desirable to have a reference system that is static with respect to the ground in each support phase. It is convenient to place the reference coordinate system in the center of the respective support polygon. That means we place the ground frame at the TCP of the respective foot in each single support phase. As the ground frame should be aligned with the floor, we use the projection of the foot poses to the floor plane. In dual support phase, we calculate the pose from the position by $p = \frac{1}{2} \cdot (p_{left} + p_{right})$ and the y-axis by $y = \frac{1}{2} \cdot (y_{left} + y_{right})$. The z-axis is the normal of the floor plane: $z = (0, 0, 1)^T$. See figure 4.2 for an example. The resulting reference frame is called the *ground frame*.

4.2.2 Controlling the body posture

The control strategy of the chest pose is straightforward: Given the reference roll angle ϕ^d and reference pitch angle θ^d compute the differences to the actual angles ϕ and θ . The main problem in a real robot is to obtain the actual global pose of this frame. The proposed method is to use a Kalman filter to estimate the pose from the joint position and accelerometers. We did not implement this method in simulation, as it is easy to obtain the exact pose from the simulator. To prevent rapid movements of the chest that cause large accelerations, a dampening controller is used. The angles $\Delta\phi$ and $\Delta\theta$ can be calculated by the following equations:

$$\Delta\dot{\phi}_C = \frac{1}{D_C}(\phi_C^d - \phi_C) - \frac{1}{T_C} \cdot \Delta\phi_C \quad (4.1)$$

$$\Delta\dot{\theta}_C = \frac{1}{D_C}(\theta_C^d - \theta_C) - \frac{1}{T_C} \cdot \Delta\theta_C \quad (4.2)$$

D_C describes the damping gain. T_C is the constant that describes how long it will take to reach the normal positions $\Delta\phi = 0$ and $\Delta\theta = 0$ respectively if there is no error.

The modified reference frame R_C^{d*} can be calculated by rotating the reference frame by the additional angles:

$$R_C^{d*} = R^d \cdot R_{RPY}(\Delta\phi_C, \Delta\theta_C, 0) \quad (4.3)$$

To get an idea how this controller compensates CoM inaccuracies consider the case where the upper

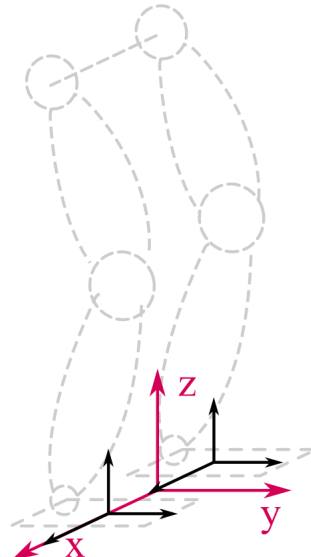


Figure 4.2: Ground frame in dual support

body is bent forward. Since our reference trajectory specifies an upright upper body pose we can assume that $\phi_C^d = 0$. Since the upper body is bent forward the roll angle ϕ will be below zero. Depending on D_C we will eventually reach $\Delta\phi_C \approx |\phi_C|$, thus the reference frame will be modified to bent backwards to compensate the wrong pose.

4.2.3 Controlling the ankle torques

Since the stabilizer only has the joint trajectory and desired ZMP trajectory as input, we need a way to compute the desired actuation torques on the ankles. The canonical way to do this would be to solve the inverse dynamics of the robot. However an accurate robot model, including correct masses and moments of inertia for each link, is needed for this. This model is not always easy to obtain and calculating the inverse dynamics of a robot with many degrees of freedom is rather slow. For this reason a simple heuristic is proposed to yield approximate torques given a reference ZMP position. However in the single support phase it is easy to calculate the *exact* actuation torque on the ankle, that is required to realize the given reference ZMP.

First we need to calculate the force in z -direction applied on the foot at the ankle p_{ankle} which we name f_g by:

$$f_g = M \cdot g \quad (4.4)$$

Where g is the gravity vector and M the mass of the robot. Given f_g acting on the ankle position p_{ankle} we can obtain the ankle torque in single support phase easily using the fact, that the torque around the ZMP is zero:

$$\begin{aligned} \tau_{zmp} &= (p_{ankle} - p_{zmp}^d) \times f_g + \tau_{ankle}^d \\ 0 &= (p_{ankle} - p_{zmp}^d) \times f_g + \tau_{ankle}^d \\ \tau_{ankle}^d &= -(p_{ankle} - p_{zmp}^d) \times f_g \end{aligned} \quad (4.5)$$

In dual support phase that matter is more complicated. Since both feet are in contact with the ground, the weight of the robot is distributed between them. If we take the forces f_R and f_L which act on the right ankle p_R and left ankle p_L respectively we know that $f_R + f_L = f_g$. Thus there exists $\alpha \in [0, 1]$ for which: $f_R = \alpha \cdot f_g$ and $f_L = (1 - \alpha) \cdot f_g$. A heuristic method for computing this alpha is the *ZMP distributor*.

The idea is to calculate the nearest points $p_{L\#}$ and $p_{R\#}$ from the ZMP to the support polygons of the feet. If the ZMP falls inside one of the support polygons, we set $\alpha = 1$ or $\alpha = 0$ respectively. If it is outside of both support polygons the ZMP is projected onto the line from $p_{L\#}$ to $p_{R\#}$ yielding the point p_α .

We can then set α to:

$$\alpha = \frac{|p_\alpha - p_{L\#}|}{|p_{R\#} - p_{L\#}|} \quad (4.6)$$

If τ_L and τ_R are the torques in the left and right ankle respectively, we can calculate the torque around the ZMP as:

$$\tau_{zmp} = (p_R - p_{zmp}^d) \times f_R + (p_L - p_{zmp}^d) \times f_L + \tau_L^d + \tau_R^d \quad (4.7)$$

As before, we assume that $\tau_{zmp} = 0$ which lets us solve 4.7 for $\tau_0 := \tau_L^d + \tau_R^d$:

$$\tau_0 = (p_R - p_{zmp}^d) \times f_R + (p_L - p_{zmp}^d) \times f_L \quad (4.8)$$

We now again apply a heuristic using the α computed before to distribute τ_0 to each ankle. First we need to transform τ_0 from the global coordinate system to a local coordinate system described by the *ground frame*. We mark all vectors in the local coordinate system with $'$. The heuristic applied is: The torque around the x -axis in each ankle is approximately proportional to the force applied at that ankle.

From that we can derive:

$$\tau_{Rx}^{d'} = \alpha \tau'_{0x} \quad (4.9)$$

$$\tau_{Lx}^{d'} = (1 - \alpha) \tau'_{0x} \quad (4.10)$$

The torque around the y -axis depends on the direction of the total torque τ'_{0y} . If the total torque acts in clockwise direction (negative sign), we can assume it will only be applied to the left foot. If the torque acts in anti-clockwise direction (positive sign), we assume it will only be applied to the right foot.

$$\tau_{Ry}^{d'} = \begin{cases} \tau'_{0y}, & \tau'_{0y} > 0 \\ 0, & \text{else} \end{cases} \quad (4.11)$$

$$\tau_{Ly}^{d'} = \begin{cases} \tau'_{0y}, & \tau'_{0y} < 0 \\ 0, & \text{else} \end{cases} \quad (4.12)$$

We can now transform the torques from our local coordinate system to the coordinate system of the corresponding foot yielding τ_L^d and τ_R^d . Now that we have obtained the reference torques, we can try to control the torque in each angle using the measured torques τ_R and τ_L . However since we assume a position controlled robot, the torque differences need to be translated into pose changes. There are three primary cases that need to be considered if we change the reference pose of a foot:

The foot is not in contact with the ground: Changing the reference pose will just affect the foot

The foot is in contact with the ground, but the contact is non-solid: If the foot has a soft contact surface (e.g. rubber) we can model the contact with the ground as springs that connect the ground with the contact points on the foot. Changing the pose of the foot will relax/compress the springs and change the contact forces accordingly.

The foot is in solid contact with the ground: Changing the reference foot pose *will not change the foot pose at all*. Instead, the pose of the rest of the robot is changed. If the foot pose is changed by the angles $\Delta\phi$ and $\Delta\theta$ all other frames of the robot will be changed by $-\Delta\phi$ and $-\Delta\theta$.

For a foot with a rubber surface we will start with a non-solid contact and transition to a solid contact, once the rubber is sufficiently compressed. [11]

To get an idea how changing the pose on such a foot with rubber surface affects the torque, consider the case of rotating the foot around its lateral axis (x -axis) in anti-clockwise direction. Since the contact with the ground is at first non-solid, we can employ the spring model. The springs at the front of the foot are compressed thus the force applied at the corresponding contact points increases. Accordingly the springs at the back are compressed less, thus the force applied to the corresponding contact points decreases. Resulting we see a increase in torque around the x -axis.

If the springs are compressed sufficiently, we can assume the contact with the floor is solid. Since the pose of the foot does not change, the increase in the joint angle in the ankle will rotate the upper body backwards. Recall the 3D-LIMP model for a moment, in that model this means our pendulum swings backwards. This will lead to an increase of the torque around the x -axis in the base of the pendulum, the ankle joint.

For rotating the foot around the y -axis the same ideas hold. As a result we see that additional foot rotation long the x - and y -axis have a proportional relationship with the torque around that axis. This motivates the definition of the controller proposed by Kajita et al. The additional rotation angles are can be calculated by the following equations:

$$\Delta\dot{\phi}_i = \frac{1}{D_{ix}}(\tau_{ix}^d - \tau_{ix}) - \frac{1}{T_{ix}} \cdot \Delta\phi_i \quad (4.13)$$

$$\Delta\dot{\theta}_i = \frac{1}{D_{ix}}(\tau_{iy}^d - \tau_{iy}) - \frac{1}{T_{ix}} \cdot \Delta\theta_i \quad (4.14)$$

Where $i \in \{R, L\}$. This again utilizes the same concept of a dampening controller that was used previously for controlling the chest frame orientation. We can use the obtained angles $\Delta\phi_i$ and $\Delta\theta_i$ to compute the modified reference frames for the feet:

$$R_i^{d*} = R_i^d \cdot R_{RPY}(\Delta\phi_i, \Delta\theta_i, 0) \quad (4.15)$$

4.2.4 Foot force difference controller

In the previous section only the ankle torque were controlled to match the reference values that were derived using the ZMP distributor. However reference values for the gravitational force that each foot exerts on the ground were also obtained. These forces are not necessarily realized. Consider the case of slightly uneven ground. If the pattern assumed a flat ground, the ankle of both feet will have the same altitude. Depending on variation of floor height, that might lead to one foot not touching the ground at all. In the case of feet with rubber soles, slight variations in floor height lead to a different compression of the soles. Both cases cause a different force acting on each foot.

If we assume the mass M of the robot and the gravity vector g are correct, we know that the reference force $f_g^d = M \cdot g$ will exactly match the force in z -direction f_g exerted by the support foot in single support. Thus in single support we can guarantee that we realize our reference force. In dual support we know that $f_L^d + f_R^d = M \cdot g$. If we apply the same reasoning as above we know that $f_L^d + f_R^d = f_L + f_R$. If we can additionally make sure that $f_L^d - f_R^d = f_L - f_R$ we can deduce that $f_L^d = f_L$ and $f_R^d = f_R$.

Since the x and y components of both $f_L^d - f_R^d$ and $f_L = f_R$ are zero we only need to control the z components. As we motivated in the beginning of this section, differences in floor height are the main cause of deviation in the force. To compensate that, the height of the ankle needs to be changed. Thus the difference in ankle height z_{ctl} was chosen to compensate the difference in forces exerted by the foot. The description of the controller again uses the concept of a dampening controller, that was used in the previous sections.

$$\dot{z}_{ctl} = \frac{1}{D_z}[(f_L^d - f_R^d) - (f_L - f_R)] - \frac{1}{T_z}z_{ctl} \quad (4.16)$$

Two methods were proposed to realize this difference in ankle height. The first method is to change the reference position of the feet in z -direction:

$$p_R^{d*} = p_R^d + 0.5 \cdot \begin{pmatrix} 0 \\ 0 \\ z_{ctl} \end{pmatrix} \quad (4.17)$$

$$p_L^{d*} = p_L^d - 0.5 \cdot \begin{pmatrix} 0 \\ 0 \\ z_{ctl} \end{pmatrix} \quad (4.18)$$

This can lead to singularities if both legs are already fully stretched, as the edge of their workspace is reached. The second method relies on an additional rotating the pelvis link. For this approach to work, the robot needs a joint that allows rotations around the anterior axis (y -axis) to keep the upper body upright. Since the robot model we used does not have this DOF, we only implemented the first approach. To circumvent singularities we chose a CoM height that guarantees knee bending while generating the reference pattern.

4.2.5 Interaction between controllers

While each controller operate independently, their effects are highly coupled. The most important coupling exists between the chest posture controller and the ankle torque controller. In case of a solid contact with the ground, the ankle torque controller will not rotate the supporting foot, but rather the body of the robot. However, this will change the posture of chest frame. The chest posture controller compensates

that and keeps the body upright. The tight coupling makes tuning the parameters D_i and T_i of the controllers difficult, as their performance depends on the other controllers. Best results were observed when the chest posture controller was tuned independently first, disabling the other controllers. Then the foot force controllers was enabled and tuned and finally the ankle torque controller was added and tuned.

4.2.6 CoM and ZMP control

The controllers specified in the previous sections can make sure, that the ZMP that is realized tracks the ZMP that would result from a perfect execution of the input pattern. However depending on how the reference ZMP was predicted, that prediction might have already been wrong. For example the ZMP Preview Control approach uses the cart-table model to predict the ZMP. That prediction can deviate significantly from the real ZMP as the model simplifies the dynamics. Thus to make sure the desired ZMP is tracked accurately, the reference ZMP needs to be adapted as well.

Kajita et al. propose a dynamic system that describes the 3D-LIMP dynamics. To model the mechanical lag they introduce a parameter T_p that specifies the ZMP delay. The state-space description of the dynamic system for the x -direction is given below. As before, the description of the dynamic system for the y -direction is analogous.

$$\frac{d}{dt} \begin{pmatrix} c_x \\ \dot{c}_x \\ p_{zmp_x} \end{pmatrix} = \overbrace{\begin{pmatrix} 0 & 1 & 0 \\ \frac{g}{z_c} & 0 & -\frac{g}{z_c} \\ 0 & 0 & -\frac{1}{T_p} \end{pmatrix}}^{=:A} \cdot \begin{pmatrix} c_x \\ \dot{c}_x \\ p_{zmp_x} \end{pmatrix} + \overbrace{\begin{pmatrix} 0 \\ 0 \\ \frac{1}{T_p} \end{pmatrix}}^{=:B} u \quad (4.19)$$

As controller a feedback controller is proposed:

$$p_x^{d*} = u = (k_1, k_2, k_3) \cdot \left[\begin{pmatrix} c_x^d \\ \dot{c}_x^d \\ p_{zmp_x}^d \end{pmatrix} - \begin{pmatrix} c_x \\ \dot{c}_x \\ p_{zmp_x} \end{pmatrix} \right] + p_{zmp_x}^d \quad (4.20)$$

To derive the corresponding gains (k_1, k_2, k_3) pole-placement with the poles $(-13, -3, \sqrt{\frac{g}{c_z}})$ was proposed. The gains can be easily computed from the poles, A and B using predefined functions in MATLAB or similar software.

4.3 Implementation

To implement the stabilizer above, a number of problems had to be solved. For one, computing the inverse kinematics is challenging. During walking the base of support depends on the foot that is in contact with the ground. For example, if the left foot is the support foot, it is considered the base and the right foot is considered the TCP. If the right foot is the support foot, the reverse is true. In dual support phase, we actually have two bases of support, which yields a parallel kinematic chain. SIMOX, the framework used to compute the inverse kinematics, describes the kinematic structure of a robot as a directed tree. Solving the inverse kinematics was initially only possible for sub-trees of that tree. Chosing the the base and the TCP freely was not possible, but it was determined by the structure in which the kinematic model was initially described.

As a first approximation, a kinematic model with the left foot as root node was used. In the case of the right foot being the support foot, this approach leads to an increased error. Consider solving the inverse kinematics for both legs using a differential solver in two steps: First from the base (the left foot) to the pelvis, then from the pelvis to the right foot. Lets assume the IK computes a perfect solution to place the pelvis link and only achieves a small pose error of $e_\alpha = 0.1^\circ$ in the pitch angle of the right foot. If the trajectory is execute, the right foot will achieve its target pose, since it is constrained by the ground contact. However the error in the right foot pose will effect all other frames of the robot. Assuming a offset of $v = (-0.5, 0, 1)^T m$ from the right foot to the pelvis link, we can compute the realized pelvis

offset as $v' = R_y(-e_\alpha) \cdot v = (-0.49825, 0, 1.00087)^T m$ Which yields 1.76mm error in x-direction and 0.87mm error in y-direction.

To solve this SIMOX was extended by a function `cloneInversed` that can compute a kinematic structure with arbitrary root placement from an existing description. For the parallel kinematic chain, it proofed sufficient to approximate it as a normal kinematic chain and constrain the base and TCP targets accordingly. However since the position of one foot will have small positioning errors, there will be some jitter introduced into the system. Integrating a solver for parallel kinematics might decrease some of the jitter observed in foot contact forces during dual support, as the constraint solver used for the simulation will only amplify this jitter.

As was the case with the components of the pattern generator, the core of the stabilizer is implemented as part of LIBBIPEDAL. A plugin integrates the stabilizer into the dynamic simulation.

4.4 Problems

When testing the stabilizer proposed by Kajita, some problems became immediately clear. The ground reaction forces in dual support are oscillating wildly. Instead of a continuous force at about $0.5 \cdot f_g$ the forces on both feet oscillate between 0 and f_g , the support foot changes in rapid successions. As outlined in section 6.1 this is a result of the constraint solver method employed by BULLET. Subsequently the measured torques on the ankles did not follow the prediction as well. These are the actual values used by the simulator, not merely sensor noise. Even when adding mean-filters to smoothen the measured torques it was not possible to extract a meaningful control signal. Besides the sequential impulse solver newer versions of BULLET support a solver based on the Featherstone algorithm. Given the scope of this thesis, integrating that solver was out of question. Thus, an alternative approach to stabilizing had to be found. However, the Featherstone solver should be implemented in future work.

4.5 Alternative approach

As a simple heuristic, we used the controllers proposed by Kajita as inspiration and replaced the force and torque feedback with the pose error of pelvis and feet frames respectively. The chest controller (Equation 4.1 and 4.2) Kajita et al. proposed for controlling the body posture were adapted to all control frames to provide a feedback on the pose error.

This yields a controller that keeps the feet pose parallel to the ground, which is important when the swing foot touches the ground. Controlling the pelvis and chest pose to follow the reference also keeps the robot upright. It is not feasible to implement this stabilizer in practice. As mentioned in section 4.2 precisely estimating the pose of a robot is not easy. While the dampening controllers can be configured to smoothen a noisy sensor signal, a high level of precision is required to ensure a correct foot posture.

Since the ZMP and CoM trajectory is not adapted, the compensation of environment disturbances is only based on a fast controller reaction to leave the reference trajectory as little as possible and the stability margins the ZMP provides. However as we will discuss in the evaluation section, this simple approach is already surprisingly resilient.

5 Push recovery

As we saw in the chapter about Stabilizers, not all disturbances can be compensated. If the disturbance reaches a certain severity, the trajectory can not be executed as planned without falling. Thus the trajectory needs to be changed radically to avoid falling. There is little hope to recover from continuous heavy disturbances, as any attempt to recover will be defeated. Thus we focus on short but severe disturbances, pushes.

The most prominent method to recover from pushes is the Capture Point. The idea is to find a point, that will guarantee that the CoM comes to a rest, if the support foot is instantaneously placed there. The push recovery implemented here uses a simplistic method based on the Capture Point.

5.1 Capture Point

Koolen et al. [12] derive the Capture Point for multiple models based on the 3D-LIPM. The simplest model is the 3D Linear Inverted Pendulum with a point contact and a massless telescopic rod. If we use the LIP equations 2.12 and 2.13 with zero input torque, we can derive that so called *orbital energy* of the pendulum. As we did in chapter 3, we will derive the equations only for one dimension. The other dimension follows analogous.

The base of the pendulum is assumed to be at the origin of the reference frame in 2.12. Since we want to specify the location of the CoM $c = (c_x, c_y, c_z)$ freely, we need to substitute c_x with $c_x - p_x$ to yield:

$$\ddot{c}_x = \frac{g}{z_c} (c_x - p_x) \quad (5.1)$$

The orbital energy E_x can be derived by subtracting the potential and kinetic energy:

$$E_x = \underbrace{\frac{1}{2} \dot{c}_x^2}_{\text{kinetic energy}} - \underbrace{\frac{g}{2 \cdot z_c} (c_x - p_x)^2}_{\text{potential energy}} \quad (5.2)$$

For the CoM to come to a rest the orbital energy E_x must be zero. Thus we can solve 5.2 to yield the x coordinate of point p that will achieve this. Since it is a quadratic equation there are two solutions:

$$p_x = x - \sqrt{\frac{z_c}{g}} \dot{c}_x \quad \text{or} \quad p_x = x + \sqrt{\frac{z_c}{g}} \dot{c}_x \quad (5.3)$$

Since it is generally desirable to chose a point that lies in the direction of the CoM motion we define the *Immediate Capture Point* as:

$$p_{ic} := c_x + \sqrt{\frac{z_c}{g}} \dot{c}_x \quad (5.4)$$

Placing the base of the pendulum (the ankle) there *instantaneously* will cause an orbital energy of zero, thus the head of the pendulum (the CoM) will stop at p_{ic} . In most cases we will not be able to move the base of the pendulum instantaneously. So we are more interested in the Immediate Capture Point in Δt seconds from now. This point can be obtained by 5.5. For a detailed derivation, we recommend the paper by Koolen et al. [12].

$$p_{ic}(\Delta t) = p_{ankle} + (p_{ic}(0) - p_{ankle}) \cdot e^{\frac{g}{z_c} \cdot \Delta t} \quad (5.5)$$

Where p_{ankle} is the current position of ankle of the support foot (the current base of the pendulum). and $p_{ic}(0)$ is the current Immediate Capture Point as calculated by equation 5.4.

5.2 Fall detection

The first important step to recover from a large disturbance is to detect it. That means we need to detect if we reached a unstable state, from which it is unlikely that we can recover only by means of the stabilizer. We can use the measured ZMP to obtain a heuristic for such states. If the ZMP is outside or on the edge of the support polygon, the Cart-Table model does not guarantee stability. However in normal operations it is likely that the ZMP will touch (or leave) the border of the support polygon for short periods of time. A simple method to filter out this noise is to define a minimum duration the ZMP as to be in an unstable state. Choosing a small value will let us react faster to disturbances, but make the method error prone. Choosing a large value will add an additional delay until we can react, but is much less prone to be triggered by mistake. An experimental evaluation yielded good results with a duration of $t = 30ms$.

5.3 Recovery

If a fall is detected, a recovery maneuver needs to be executed. In single support phase, that means we need to place the swing foot at the capture point. In dual support phase we try to move the support foot that is closest to the capture point. Recall that the base of the pendulum coincides with the ZMP in our model view. Thus if the resulting support polygon includes the capture point, the position will be stable. Since the motor velocities are limited, we need a minimal amount of time t_{min} to place the foot in the desired location. Thus instead of using the Immediate Capture Point, we use the future Immediate Capture Point $p_{ic}(t_{min})$ to derive the desired location. A value of $t_{min} = 0.35s$ yielded good results.

5.4 Implementation

The stabilizer that is outlined in chapter 4.2 was extended to call the fall detection module in each iteration of the control loop. If an unstable state is reached, the recovery module overrides the normal trajectory of the stabilizer. After completing the recovery maneuver, the robot remains in the given position. Resuming the original pattern requires planning a dynamically stable transition trajectory. This is left for future work.

6 Dynamic Simulation

To evaluate the generated trajectories a simulator for the dynamics was developed. The simulator was build on the SIMDYNAMICS framework that is part of SIMOX. SIMDYNAMICS uses BULLET PHYSICS as underlying physics framework. A big part of the work on the simulator was spend on configuring the parameters and finding flaws in the physics simulation. Thus, the simulator includes a extensive logging and visualization framework that measures all important parameters of the simulation. For visualizing and analysing the measurement the Open Source tools IPYTHON, NUMPY and PANDAS were used.

6.1 Simulating rigid body dynamics

Physical simulation in general can be divided into discrete methods and continuous methods. Discrete simulators only compute the state of the system at specific points in time, while continuous simulators are able to compute the state of the system at any point in time. While continuous simulation is the more flexible approach, it quickly becomes impractical with a high number of constraints. A large amount of differential equations need to be solved. Since it is hard to obtain analytical solutions for most differential equations, numerical methods need to be used, which are slow. In contrast, discrete simulation methods only compute simulation values for specific time steps. This exploits the observation that we will typically query the state of the physics engine only at a fixed rate anyway, e.g. at each iteration of our control loop. Rather than solving the differential equations that describe the physical system in each step, a solution is derived from the previous simulation state.

In a physical system we can typically find two kind of forces: Applied forces and constraint forces. Applied forces are the input forces of the system. Source of applied forces are for example gravity and objects like springs. Constraint forces are fictional forces that arise from constraints we impose on the system: Non-penetration constraints, friction constraints, position constraints of joints or velocity constraints for motors. Mathematically we can express such constraints in the form: $C(x) = 0$ or $\dot{C}(x) = 0$ in the case of equality constraints, or as $C(x) \geq 0$ or $\dot{C}(x) \geq 0$ in the case of inequality constraints. x is typically a vector in Cartesian space.

For example the position constraint of a joint p connected to a base p_0 with distance $r_0 = \|p - p_0\|$ would be: $C(p) = \|p - p_0\|^2 - r_0^2$. If p is moving with a linear velocity v a constraint force F_c is applied to p to maintain this constraint. We can view C as a transformation from our Cartesian space to the constraint space. Thus, by computing the Jacobian J of C we can relate velocities in both spaces. Furthermore, we can relate constraint space forces λ with Cartesian space forces using the transpose of the Jacobian. Thus, if we can find the constraint space force λ that is needed to maintain this constraint, we can compute F_c using $F_c = J^T \lambda$. Computing this constraint space forces is the task of the constraint solver.

The constrained solver used by BULLET, and thus the constraint solver used for simulating the patterns in this thesis, is a sequential impulse solver. To make some calculations easier, a SI solver works with impulses and velocities, rather than forces and accelerations. Impulses and forces can be easily transformed in each other as $P = F \cdot T$ where P is the impulse and T the time step size. A sequential impulse solver tries to compute the constraint force (in this case rather impulse) λ for each constraint *separately*. For each constraint the following steps are executed:

1. Compute the velocity that results from *applied forces* on the body
2. Calculate constraint force to satisfy the velocity constraint
3. Compute new velocity resulting from constraint force *and* applied force on the body
4. Update position of the body by integrating velocity: $p[n+1] = p[n] + v \cdot T$

Of course this might not lead to a global solution, as satisfying a constraint might violate a previously solved one. The idea is to repeatedly loop over all constraints, so that a global solution will be reached. The quality of this method relies on how often this loop is executed. Consider the case of a kinematic chain. Moving a link will always violate at least one position constraint. A lot of iterations are needed to yield good results in this case. It becomes even worse in the case of a parallel kinematic chain, that is in contact with the ground. This is the case for a bipedal robot in dual support stance. Solving a non-penetration constrain on either end will invalidate the position constraint of the next link. In turn, the position constraint of each link needs to be updated until the other end of the kinematic chain is reached. If the non-penetration constraint is violated again for the other end, the whole process starts again in reverse direction. This leads to oscillations that need a high number of iterations to level off to an acceptable level. Despite these inaccuracies, by using enough solver iterations an overall usable systems can be derived. However, the velocities will still have a small random error in each simulation step. This poses a major problem when trying to measure accelerations, as the random error causes them to accelerate wildly. This circumstance needs to be taken into account when dealing with values derived from the acceleration (e.g. the ZMP), as mean-filters might be necessary.

6.2 Practical challenges of physics simulations

While walking only the feet of the robot are in contact with the ground. Thus, the stability of the whole robots depends on the contact of the feet with the floor. Especially in single support phase that area is very small with regard to the size of the robot. For that reason the accuracy of ground contact forces and friction is of utmost importance for the quality of the simulation. In general, three classes of errors need to be eliminated to get a good simulation:

1. Incorrectly configured parameters, such as fictions coefficients and contact thresholds
2. Numerical errors
3. Inherent errors of the method

As outlined in section 6.1, the physics of the system are formulated as input forces and constraints that need to be solved for the constraint forces. Since BULLET uses the iterative approach described in section 6.1, it is important to use a sufficient amount of iterations for each simulation step. Another important parameter is the time step of each simulation step. Through experimental evaluation, a simulation with 2000 solver iterations and a time step size of $1ms$ was sufficiently stable. However, since the number of iterations is very high and a lot of time steps are calculated during the simulation, numeric errors become significant. That made is necessary to use double precision floating point numbers for the values used during simulation.

To decide which contact constraints are active for which points, BULLET must solve for object collisions. Depending on the objects involved different algorithms are used to calculate the contact points. Major gains in accuracy could be observed by replacing the feet and the floor with simple box shapes, instead using mesh based models.

6.3 Implementation

The simulator was designed to load arbitrary motions in the MMM format and replay them. Additional stabilization algorithms can be applied depending on additional information provided in the MMM motions. These stabilization algorithms are implemented by sub-classing `TrajectoryController`. They are invoked in each simulation step.

Currently three controllers are implemented. A controller based on the stabilizer proposed by Kajita (as outlined in section 4.2), a simple heuristic stabilizer (outlined in section 4.5) and a controller that just plays back the specified walking pattern. Each control algorithm is invoked in the same cycle time as the reference walking pattern.

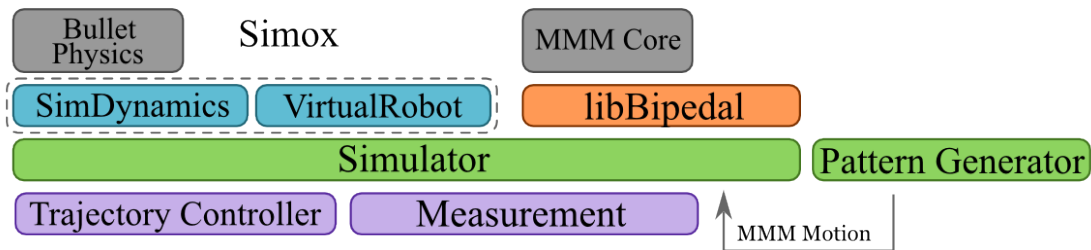


Figure 6.1: Achitechture of the simulator

The resulting, possibly modified, joint angles are then interpolated using cubic splines. This ensures a smooth velocity profile and mitigates destabilizing oscillations caused by large velocity changes. The interpolated angles are send via SIMDYNAMICS to the corresponding motors. Since the motor implemented in BULLET are velocity controlled, PID based motor controllers were added to SIMDYNAMICS. They control the motor velocities to compensate position errors. The motors implemented in BULLET do not limit the motor velocity and acceleration. This is not consistent with real motors, thus limits for velocities and acceleration were introduced to SIMDYNAMICS, that can be configured per joint.

The graphical user-interface supports the visualization of measured and desired values for CoM, Immediate Capture Point, ZMP, ankle torque, and ground reaction forces. The best-case trajectory can be visualized as an overlay robot (“phantom robot”). Figure 6.2 shows some of the supported visualizations.

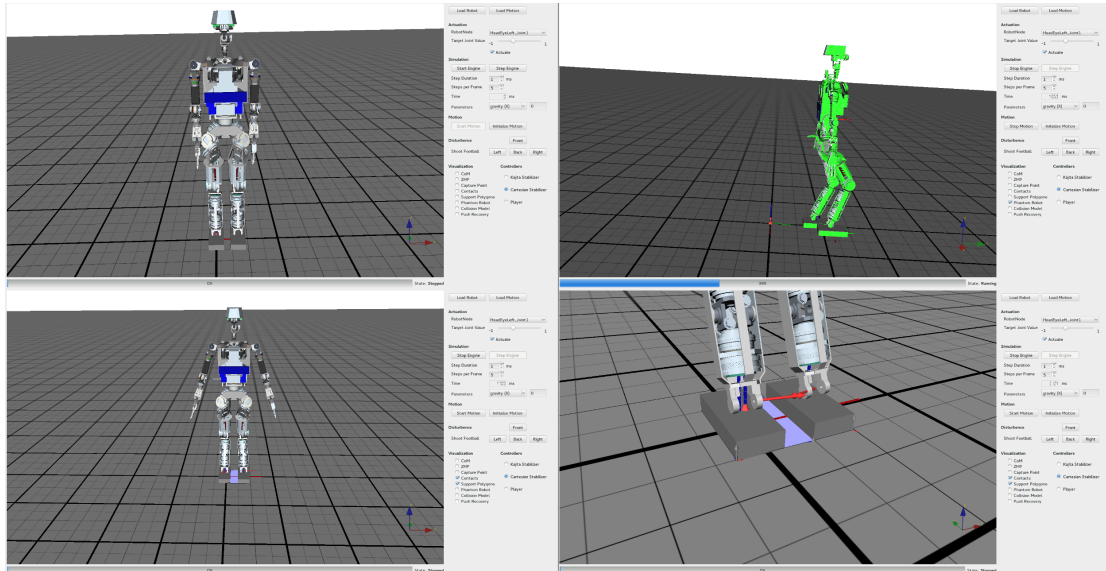


Figure 6.2: GUI of the simulator. Top left: Before starting the physics engine. Top right: Robot with best-case “phantom” overlay. Bottom left: Robot standing with support polygone visualization. Bottom right: Close-up of the support polygone, ankle torques and ground reaction forces.

An important part of the simulation is the generation of measurements that can be carefully evaluated offline or displayed in the visualization. For this purpose a modular measurement component was added to the simulator. An important design goal was to keep the measurement component as simple to extend and maintain as possible. Each module measures a specific set of values and writes them, indexed by the corresponding timestamp, to its log file. As output format the well known plain text format CSV was used. The visualization can query the measurement components directly to get the newest values to be displayed. For example the ZMP module measures the actual ZMP and also provides an interface to query the trajectory ZMP and the reference ZMP that was provided as input for the pattern generator. Thus all three values can be displayed in the visualization and easily compared later by analysing the log file. Since the goal was to keep the component as simple as possible, we use existing well known tools for analyzing the generated log files. Some small helper scripts are provided to make it easier to load

the data into the time series analysis framework PANDAS. PANDAS interfaces with the popular plotting framework MATPLOTLIB to display plots of the data. IPYTHON is used to easily run the analysis and display the results in a browser window. Most plots of simulated patterns found in this thesis can be generated automatically for every simulation.

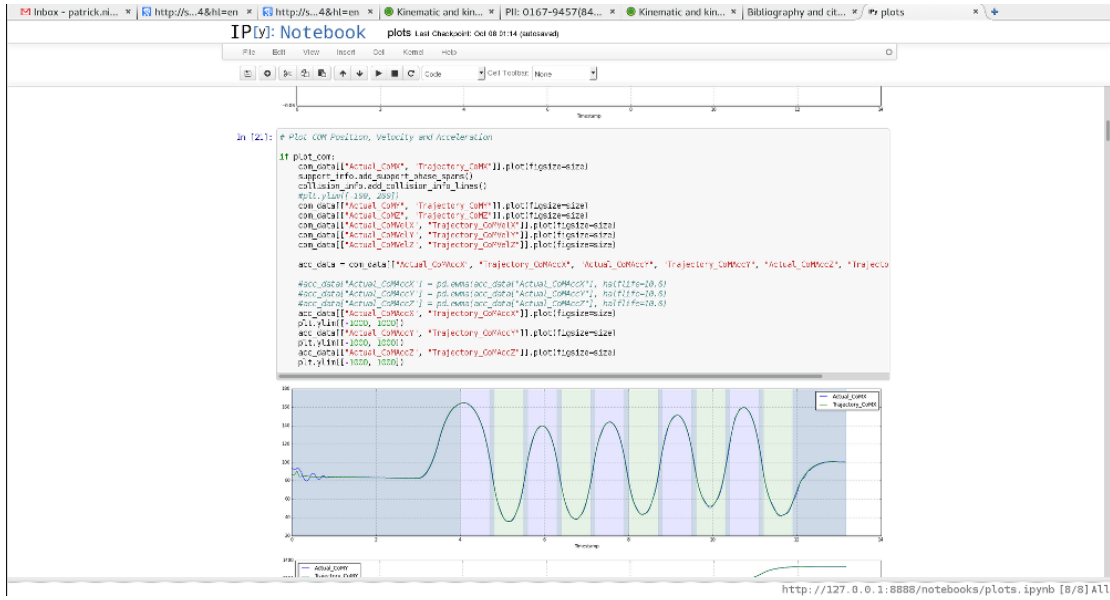


Figure 6.3: Screenshot of ipython showing plots of the CoM obtained by a simulation

7 Experimental Evaluation

To test the performance of the stabilizer against simple pattern playback, both walking straight and walking in circle were tested. To simulate further disturbances, the simulation shoots a football at the robot. In the unstabilized case, only the joint trajectory that is generated by the pattern generator is interpolated and replayed. In the stabilized case the alternative stabilizer described in section 4.5 is used.

7.1 Undisturbed walking

7.1.1 Walking in a straight line

The first scenario is walking in a straight line for 10 steps, which is shown by figure 7.1.

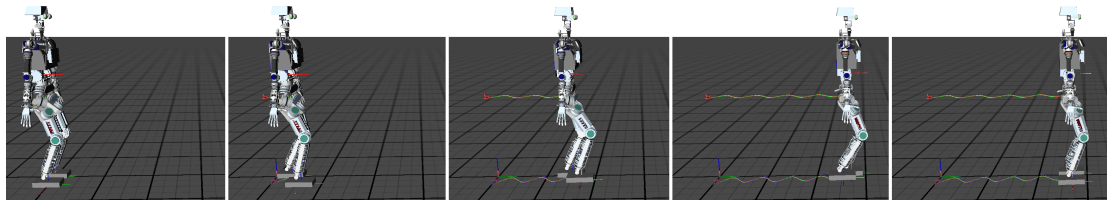


Figure 7.1: Frames of undisturbed straight walking. The desired and realized CoM trajectory is shown as green and red line respectively. [13]

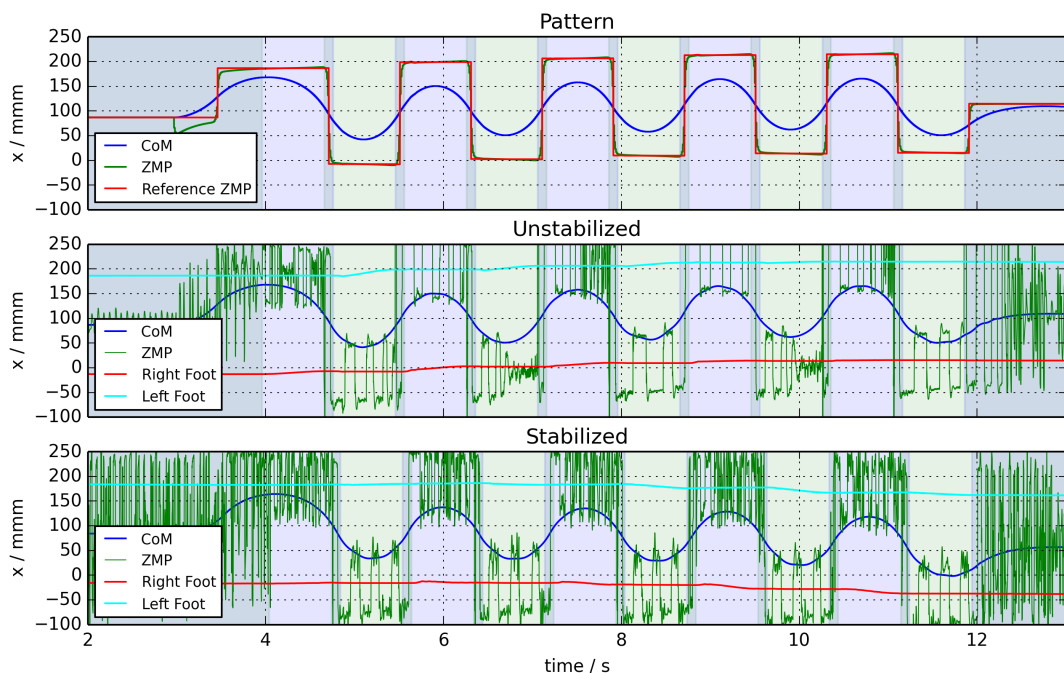


Figure 7.2: CoM and ZMP as specified by the pattern (top) and actual realized values (middle and bottom). All coordinates in the global reference frame. The background indicates the supporting foot. Blue corresponds with the right foot and green with the left foot.

Figure 7.2 shows the desired and realized CoM and ZMP trajectories in both cases. As can be seen, the ZMP deviates significantly from the desired trajectory and oscillates between both edges of the support polygon. We believe this is caused by the problems outlined in section 6.1. Consider figure 7.3 which shows the desired CoM acceleration in comparison to the realized acceleration.

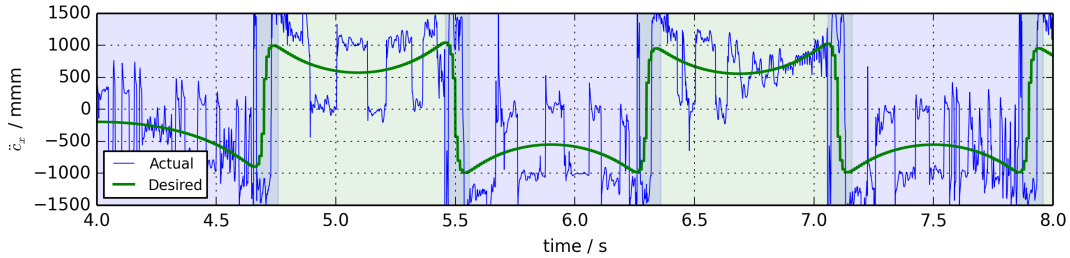


Figure 7.3: Acceleration of the CoM in x -direction.

However the foot remains in full ground contact and friction forces are applied accurately. Thus dynamically stable walking is realized for both unstabilized and stabilized walking. See figure 7.4 for the contact forces that are applied to each foot while walking. The forces oscillate due to simulation error. However the mean values meet the expectations of the gravity force vector.

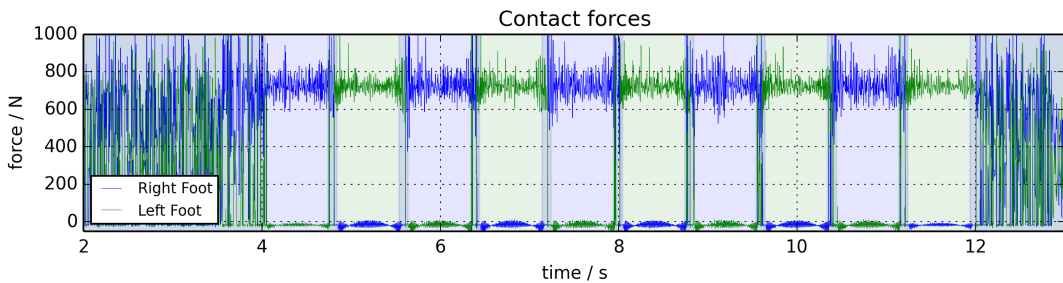


Figure 7.4: Contact forces in z direction for both feet.

Figure 7.5 depicts the ankle torques that are applied to each feet. Please note the rapid change in sign during single support. We believe this is caused by BULLETS method of applying contact forces. Contact forces are always applied to the contact point with the deepest penetration into the floor. In flat ground contact the penetration depth of contact points on the edge of the support polygon is almost the same. Small errors lead BULLET to alternate between contact points on opposite sides of the support polygon. We hope that a more stable Featherstone constraint solver will produce more accurate contact forces and ankle torques.

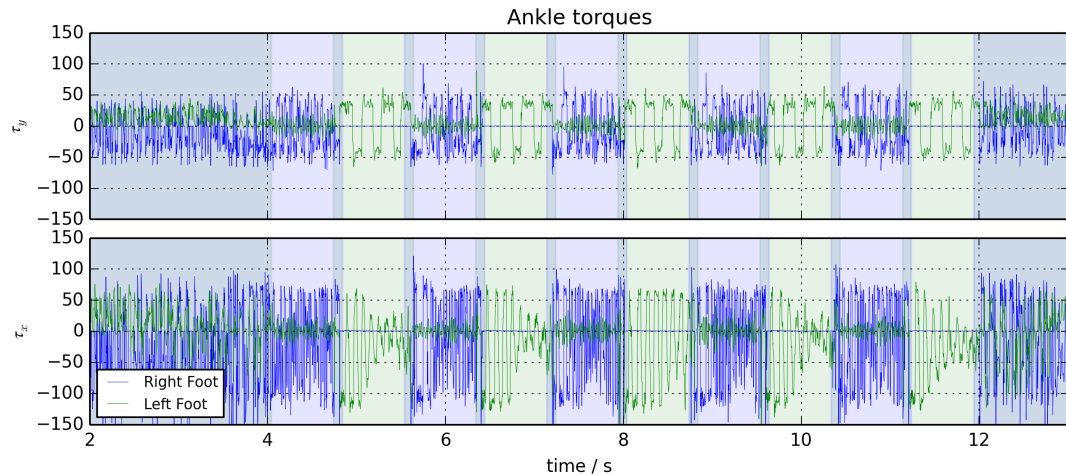


Figure 7.5: Ankle torques along the x and y axis for both feet.

An interesting way to compare the trajectory executed by ARMAR 4 to walking in humans is to use the angular momentum around the CoM. See figure 7.6 for the angular momentum trajectories as measured in test subjects by Laturnus [14] in her Bachelor's Thesis. Note the similarities to the angular momentum that is realized in the simulation in figure 7.7

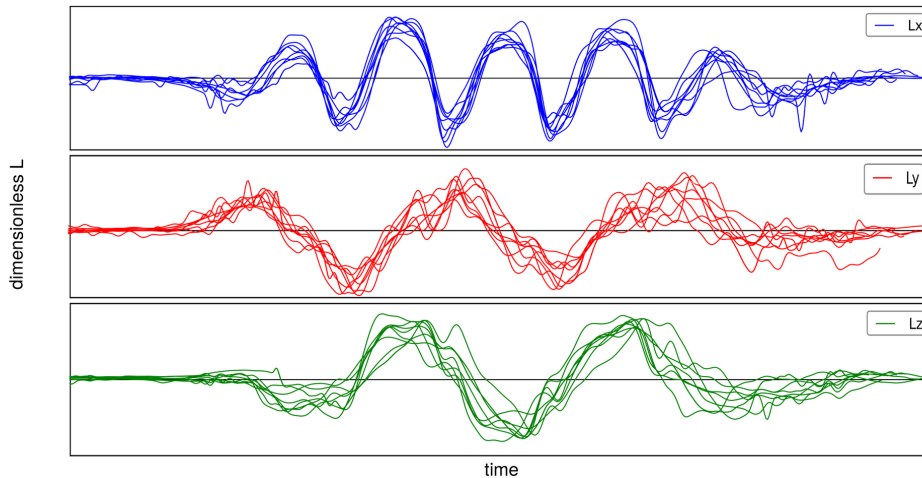


Figure 7.6: The angular momentum as measured on test subjects for straight walking by Laturnus [14]

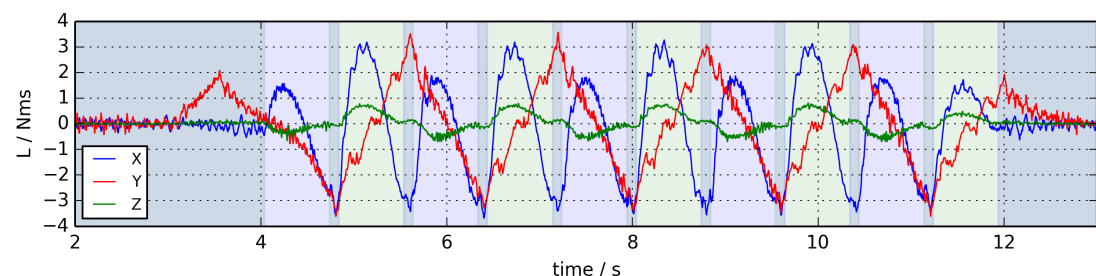


Figure 7.7: The angular momentum as measured in the simulation while walking straight.

Immediately clear are the more pronounced sharp minima and maxima of the y -component of the angular momentum. This is probably caused by the missing toe/heel lift-off and strike down phases, as

the foot is kept parallel to the floor at all times.

7.1.2 Walking in a circle

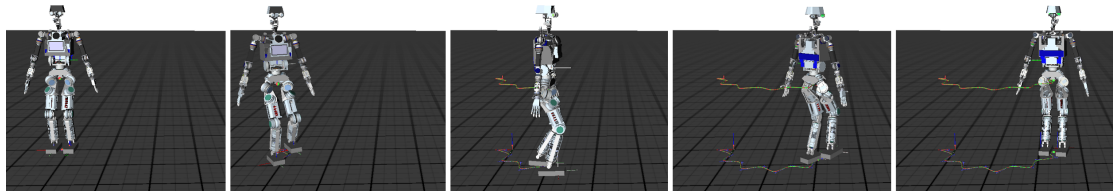


Figure 7.8: ARMAR4 walking in a half circle in 12 steps. [15]

Figure 7.8 shows the simulation of unstabilized walking in a circle. The robot walks in 12 steps in an arc of 180° and 0.5 m radius. As you can be seen, the desired 180° turn is not realized completely. Due to the chest rotation following the tangent of the circle, a torque around the yaw-axis is exerted on the foot. Recall that during pattern generation we assumed that this torque is zero. Since we do not correct this disturbance the trajectory deviates significantly. See figure 7.9 for the realized ZMP distribution and CoM trajectory for both unstabilized and stabilized walking. The unstabilized trajectory will get unstable towards the end of the trajectory. However the stabilized trajectory remains stable.

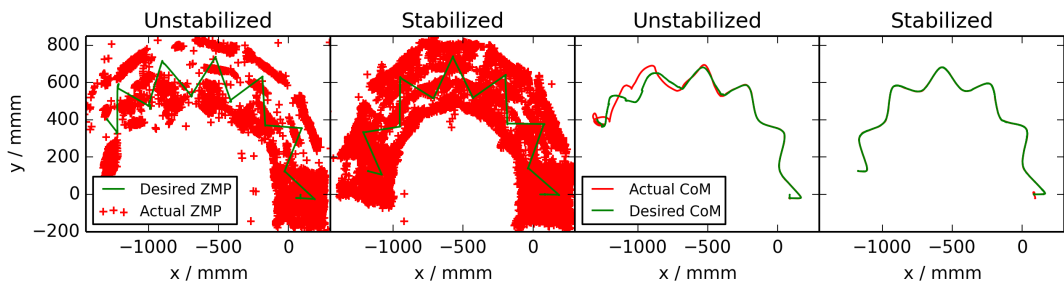


Figure 7.9: Walking in a circle. ZMP (left) and CoM (right) as specified by the pattern and the actually realized values. Each for the unstabilized and stabilized case.

7.2 Disturbed walking

Applying a short push to the chest, back, left shoulder and right shoulder was used as scenario to test the performance of the stabilizer under disturbance. The results are compared with the performance of the unstabilized trajectory. Figure ?? shows the simulation for a push to the chest.

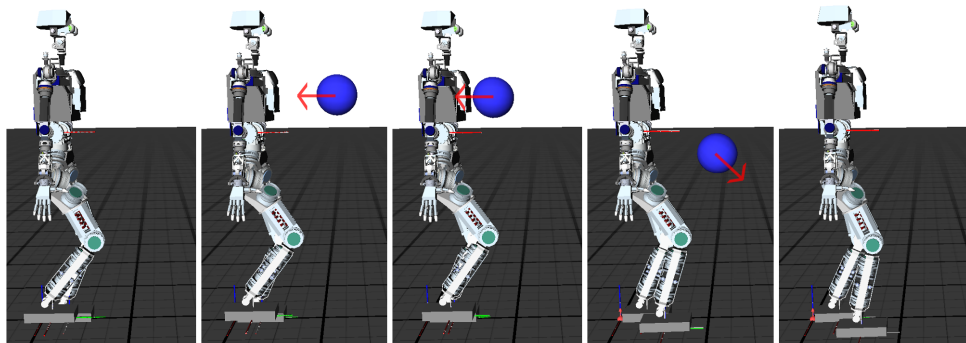


Figure 7.10: ARMAR4 getting hit by a ball at chest height. Red arrows show approximate direction of the ball velocity vector. [16]

To simulate a push, a ball with a radius of 11cm and weight of 450g (FIFA football) is shoot from 1 meter distance at the chest. See figure 7.11 for the realized CoM and ZMP trajectories. The point of impact is denoted as red lines. The unstabilized trajectory becomes unstable and leads to a fall at $t = 7\text{s}$. The stabilized trajectory is noticeable disturbed, as the yaw momentum is not compensated, but remains stable.

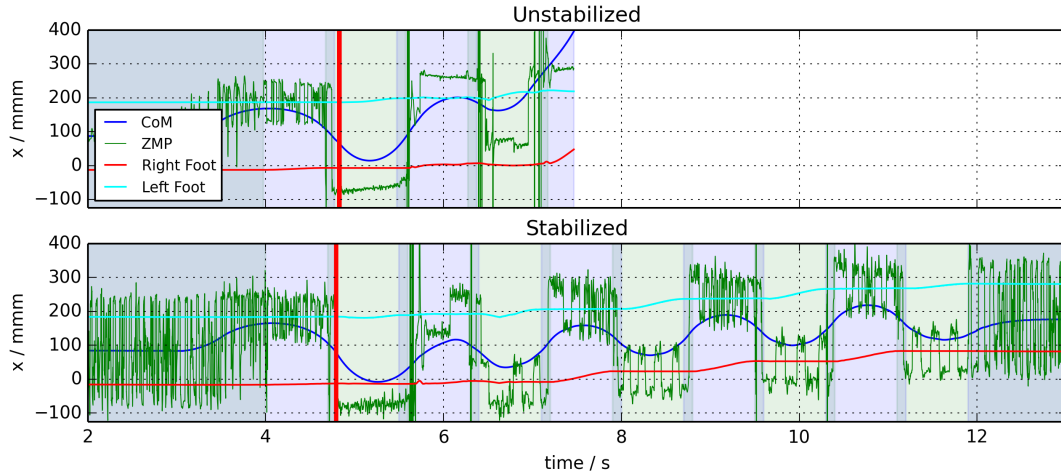


Figure 7.11: The actually realized CoM and ZMP values after a ball collision in the chest. All coordinates in the global reference frame. Red lines denote the point of impact.

Figure 7.12 shows the realized ZMP and CoM after an impact in the back. The unstabilized trajectory does not lead to falling in this case, but the trajectory of the ZMP indicates a rather unstable trajectory.

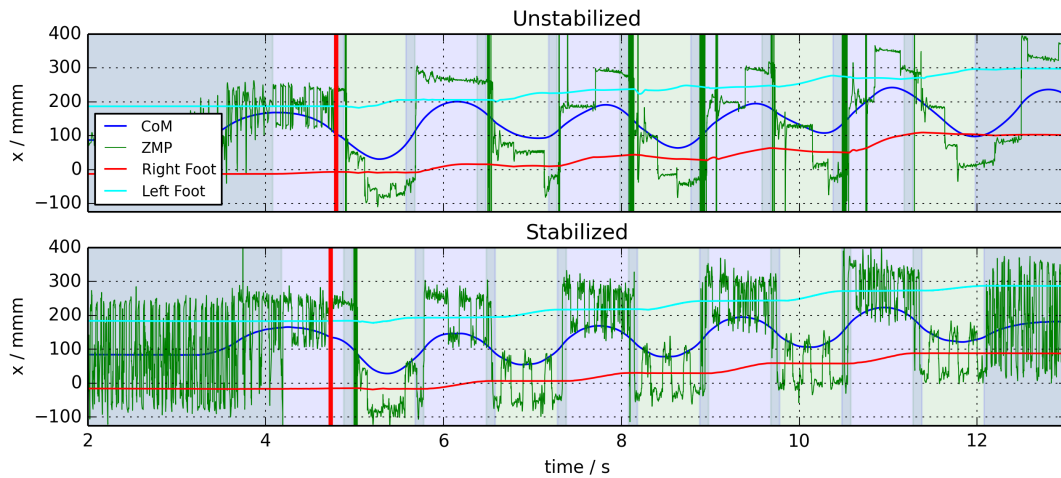


Figure 7.12: The actually realized CoM and ZMP values after a ball collision in the back.

Similar results can be observed for disturbances on the left (see figure 7.13) and right shoulder (see figure 7.14). In both cases the disturbance leads to falling in the unstabilized case.

Figure 7.15 show the impact of the push to the chest on the immediate capture point. The capture point shifts rapidly in the direction of the disturbance. This property will be utilized to derive a capture position for push recovery.

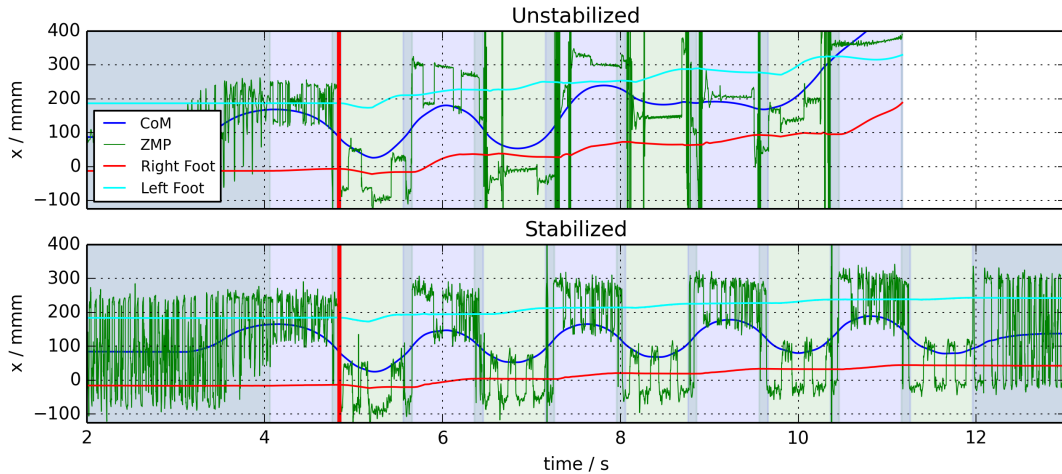


Figure 7.13: The actually realized CoM and ZMP values after a ball collision in the left shoulder.

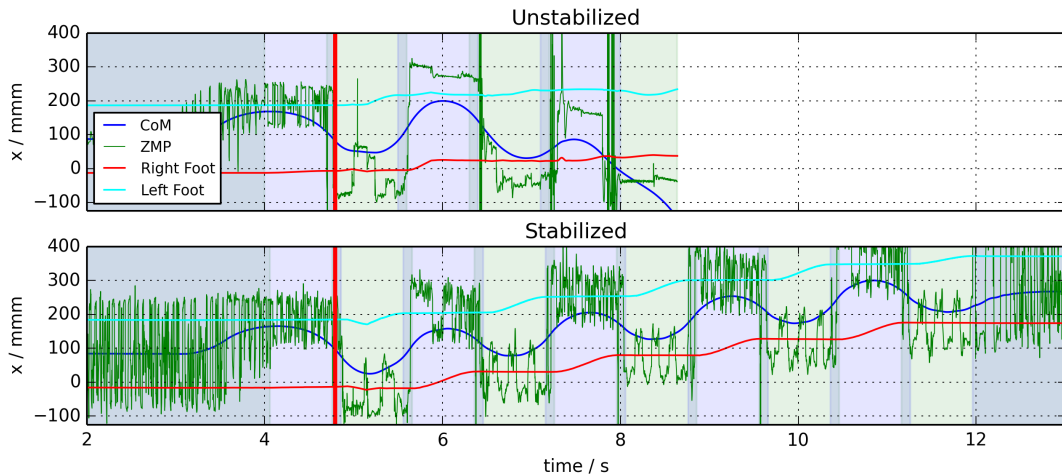


Figure 7.14: The actually realized CoM and ZMP values after a ball collision in the right shoulder.

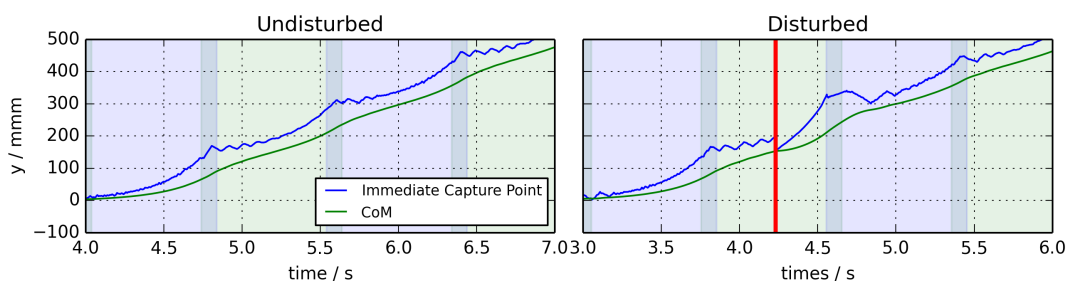


Figure 7.15: Impact of the disturbance on the immediate capture point. Red lines denote the point of impact.

7.3 Push recovery

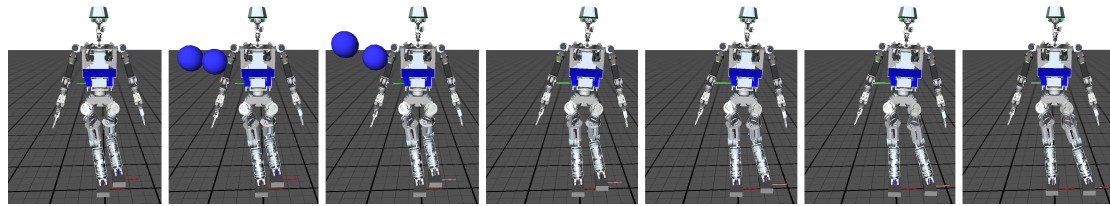


Figure 7.16: ARMAR4 getting hit by two balls at the left shoulder.

The performance of the push recovery was evaluated with a simple best-case scenario. The robot is balancing on the left foot and is pushed on the left shoulder. Most notably this scenario was used to demonstrate the push recovery based on the Capture Point implemented in the IHMC/Yobotics Biped. [17]. While the push recovery implemented is able to recover from any position, with the current method it is not reliable in the general case. There are multiple reasons for this. For one, the fall detection is not very reliable. Another reason is that the speed limits of the leg joints impose a maximum velocity for the foot movement. So not only needs the target position to be reachable, it also needs to be reachable in a short amount of time. As above a football is used as source of disturbance. Figure 7.16 shows a recovery maneuver from a push to the left shoulder.

See figure 7.17 for a trajectory of the recovery maneuver. You can see that the Immediate Capture Point jumps at the point of impact. The push recovery is activated 0.3s after the impact as the fall detection threshold is reached. You can see that the foot does not reach the desired x -coordinate. This is caused by the capture foot hitting the floor earlier than planned. However the capture point is successfully moved back into the support polygon.

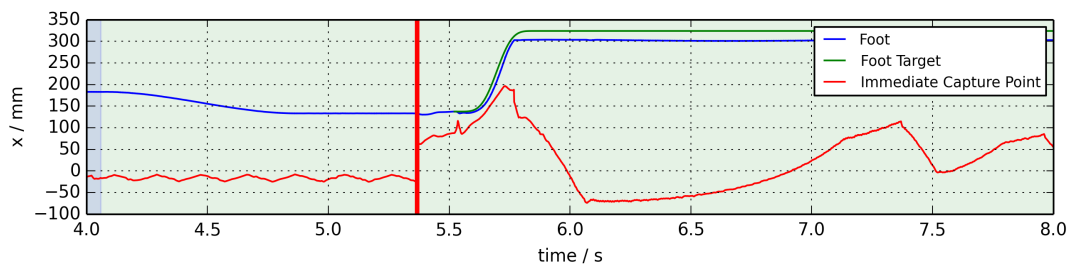


Figure 7.17: Recovery maneuver as executed for a push on the left shoulder while standing on the left foot.

8 Conclusion and future work

the design and implementation of a software framework for bipedal humanoid walking were presented. Building on an implementation by Ömer Telemz, a generator for walking pattern using ZMP Preview Control was developed. To test the resulting patterns a dynamic simulation for walking was build. The simulation utilizes the SIMDYNAMICS framework contained in SIMOX. The simulation was extended by real-time controllers for stabilization and push recovery. To facilitate easy integration into other software projects all methods presented here are implemented in a shared library LIBBIPEDAL. LIBBIPEDAL is independent of the dynamic simulation and only depends on VIRTUALROBOT for computing forward and inverse kinematics.

Evaluation showed that stable walking could be realized in simulation. By applying a stabilizer the trajectories remained stable, even when faced with disturbances. Falling was avoided by initiating a push recovery mechanism based on the Capture Point.

Since accuracy of the dynamic simulation suffered severely by using the Sequential Impulse Solver method, it should be replaced by a solver based on the Featherstone method. The improved accuracy should make a torque feedback more viable and enable to actually use the stabilizer based described and implemented in 4.2.

The pattern generator and stabilizer only realize basic walking that is notably different to human walking. For one the knees remain bent at all times, the center of mass stays at the same height and the toe joint is not used. A follow up paper [5] extends the methods implemented here to include the toes. The realized walking trajectories seem to be more natural.

Englsberger et al. [18] propose a pattern generator based on the Immediate Capture Point instead of the ZMP. Comparing the performance of both approaches could be worthwhile.

As the evaluation of the circular trajectory shows, the yaw moment exerted on the foot can cause severe disturbances. To better deal with trajectories that include turns or arm movements, the resulting torque should be compensated. Kim et al.[19] propose to move the arms around the roll axis to compensate for yaw momentum.

Another interesting approach is to use the angular momentum around the center of mass as proposed by Kajita et al. [20] and extended by Komura et al. [21] as control input.

The push recovery implemented is very basic. The placement of the foot to recover from a push does not consider collisions with the environment. Also, after executing a push recovery step, the original trajectory can not be resumed. To enable that, online planning of dynamically stable motions needs to be integrated. Also the foot is placed at the exact location of the future capture point. However it suffices to place the foot in a way to include the capture point. In most cases this would require a lot less foot movement. Moving the leg to the target point also changes the velocity of the CoM, thus it changes the location of the capture point. To compensate for this, the capture point should be tracked using a controller instead of using a static future capture point.

Bibliography

- [1] C. L. Vaughan, B. L. Davis, and J. C. O'connor, *Dynamics of human gait*. Human Kinetics Publishers Champaign, Illinois, 1992. 1
- [2] Y. Ogura, K. Shimomura, H. Kondo, A. Morishima, T. Okubo, S. Momoki, H.-o. Lim, and A. Takanishi, "Human-like walking with knee stretched, heel-contact and toe-off motion by a humanoid robot," in *Intelligent Robots and Systems, 2006 IEEE/RSJ International Conference on*, pp. 3976–3981, IEEE, 2006. 2
- [3] S. Kajita, M. Morisawa, K. Miura, S. Nakaoka, K. Harada, K. Kaneko, F. Kanehiro, and K. Yokoi, "Biped walking stabilization based on linear inverted pendulum tracking," in *Intelligent Robots and Systems (IROS), 2010 IEEE/RSJ International Conference on*, pp. 4489–4496, IEEE, 2010. 2, 14
- [4] K. Miura, M. Morisawa, F. Kanehiro, S. Kajita, K. Kaneko, and K. Yokoi, "Human-like walking with toe supporting for humanoids," in *Intelligent Robots and Systems (IROS), 2011 IEEE/RSJ International Conference on*, pp. 4428–4435, IEEE, 2011. 2
- [5] S. Kajita, K. Miura, M. Morisawa, K. Kaneko, F. Kanehiro, and K. Yokoi, "Evaluation of a stabilizer for biped walk with toe support phase," in *Humanoid Robots (Humanoids), 2012 12th IEEE-RAS International Conference on*, pp. 586–592, IEEE, 2012. 2, 34
- [6] S. Kajita, F. Kanehiro, K. Kaneko, K. Yokoi, and H. Hirukawa, "The 3d linear inverted pendulum mode: A simple modeling for a biped walking pattern generation," in *Intelligent Robots and Systems, 2001. Proceedings. 2001 IEEE/RSJ International Conference on*, vol. 1, pp. 239–246, IEEE, 2001. 3, 5, 8
- [7] M. S. Orendurff, A. D. Segal, G. K. Klute, J. S. Berge, E. S. Rohr, and N. J. Kadel, "The effect of walking speed on center of mass displacement," *J Rehabil Res Dev*, vol. 41, no. 6A, pp. 829–34, 2004. 4
- [8] B. Siciliano and O. Khatib, *Springer handbook of robotics*. Springer, 2008. 6
- [9] S. Kajita, F. Kanehiro, K. Kaneko, K. Fujiwara, K. Harada, K. Yokoi, and H. Hirukawa, "Biped walking pattern generation by using preview control of zero-moment point," in *Robotics and Automation, 2003. Proceedings. ICRA'03. IEEE International Conference on*, vol. 2, pp. 1620–1626, IEEE, 2003. 8, 12
- [10] T. Katayama, T. Ohki, T. Inoue, and T. Kato, "Design of an optimal controller for a discrete-time system subject to previewable demand," *International Journal of Control*, vol. 41, no. 3, pp. 677–699, 1985. 10, 12
- [11] S. Kajita, T. Nagasaki, K. Kaneko, K. Yokoi, and K. Tanie, "A running controller of humanoid biped hrp-2lr," in *Robotics and Automation, 2005. ICRA 2005. Proceedings of the 2005 IEEE International Conference on*, pp. 616–622, IEEE, 2005. 17
- [12] T. Koolen, T. De Boer, J. Rebula, A. Goswami, and J. Pratt, "Capturability-based analysis and control of legged locomotion, part 1: Theory and application to three simple gait models," *The International Journal of Robotics Research*, vol. 31, no. 9, pp. 1094–1113, 2012. 21
- [13] P. Niklaus, "Demonstration armar iv walking for 10 steps." http://youtu.be/lUoGN_dhkBA, 2014.

- [14] S. Laturnus, “Analysis of angular momentum in human walking,” 2014. 29
- [15] P. Niklaus, “Demonstration armar iv walking in a half circle.” <http://youtu.be/voyzw6fLvWc>, 2014. 30
- [16] P. Niklaus, “Demonstration armar iv walking stabilized with frontal push.” <http://youtu.be/wuT4HqPw6uc>, 2014. 30
- [17] J. Pratt, “Demonstration of the ihmc/yobotics biped.” <http://youtu.be/BmdeoIDf8HA>, 2009. 33
- [18] J. Englsberger, C. Ott, M. A. Roa, A. Albu-Schaffer, and G. Hirzinger, “Bipedal walking control based on capture point dynamics,” in *Intelligent Robots and Systems (IROS), 2011 IEEE/RSJ International Conference on*, pp. 4420–4427, IEEE, 2011. 34
- [19] Y. Kim, B. Lee, J. Yoo, S. Choi, and J. Kim, “Humanoid robot hansaram: Yawing moment cancellation and zmp compensation,” in *Proceedings of AUS International Symposium on Mechatronics*, pp. 19–21, 2005. 34
- [20] S. Kajita, K. Yokoi, M. Saigo, and K. Tanie, “Balancing a humanoid robot using backdrive concerned torque control and direct angular momentum feedback,” 34
- [21] T. Komura, H. Leung, S. Kudoh, and J. Kuffner, “A feedback controller for biped humanoids that can counteract large perturbations during gait,” in *Robotics and Automation, 2005. ICRA 2005. Proceedings of the 2005 IEEE International Conference on*, pp. 1989–1995, IEEE, 2005. 34